博士論文

Developing ultrafast methods of synthesis and post-synthesis modification

toward highly functionalized zeolite materials

（ゼオライトの高機能化に向けた高速合成及び後処理手法の開発）

彭策

（ホウ　サク）

Department of Chemical System Engineering

The University of Tokyo

Dissertation Committee

Toru Wakihara, Associate Professor (Supervisor)
Department of Chemical System Engineering
The University of Tokyo

Masaru Ogura, Professor
Department of Chemical System Engineering
The University of Tokyo

Atsusi Shimojima, Professor
Department of Applied Chemistry
Waseda University

Kazuhiro Takanabe, Professor
Department of Chemical System Engineering
The University of Tokyo

Masashi Okubo, Associate Professor
Department of Chemical System Engineering
The University of Tokyo

Table of Contents

Chapter 1 General Introduction

1.1 Overview on structures and applications of zeolite materials

A traditional definition of zeolite is crystalline aluminosilicate or silica polymorph constructed from corner-sharing TO_4 (T=Si and Al) tetrahedra forming a three-dimensional framework with uniformly sized pores of molecular dimensions. Currently the term of zeolite generally refers to the corner sharing network of tetrahedrally coordinated atoms not limited to Si and Al. Independent of the compositions (Si, Al, P, Ga, Ge, B, Be, etc.), zeolite materials comprise of 244 framework types. For each type, a three-capital-letter code is assigned to describe their network characters, for example, MFI, FAU, *BEA and etc.

Based on the primary building unit of TO_4 tetrahedra, zeolite frameworks can be thought of as being made of finite or infinite components such as secondary building units (SBU) and polyhedral. The typical description of different zeolite structures containing characteristic SBUs can be found on the website of international International Zeolite Association (IZA, http://www.iza-structure.org/data-bases/). Figure 1.1 shows the development of zeolite structures from the primary TO_4 units.[1]
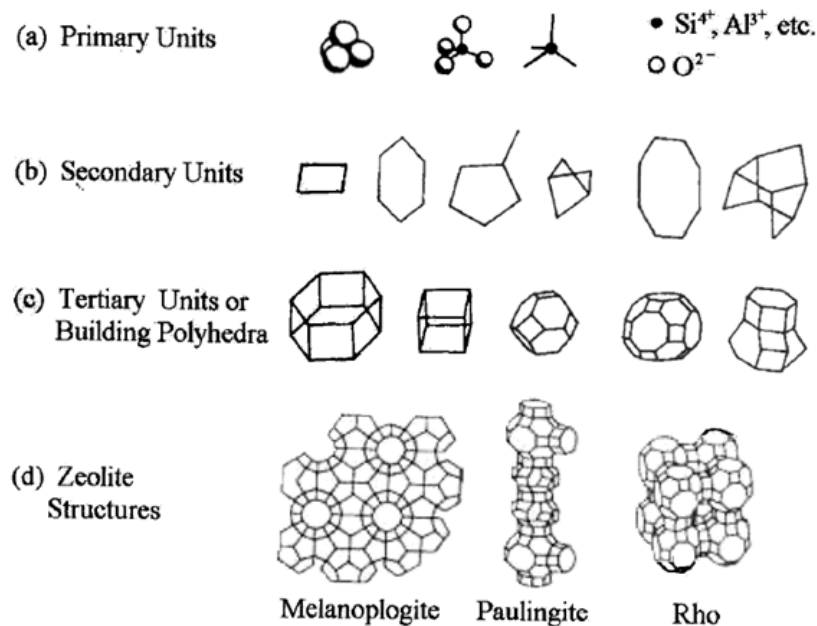
Figure 1.1 Development of zeolite structures.[1]

In addition to the intensified zeolite structures, the unique properties of zeolite materials including the shape-selectivity and acidity allowed their wide applications in industrial areas such as catalysis, gas separation, and ion-exchange fields (Figure 1.2).[2]

- *Catalysis*. The main areas of zeolite catalysts are *acid-* and *redox-* catalysis. In the former, the zeolite structures, Brønsted acid sites, Lewis acid sites are often exploited in petrochemical industry.[3] For example, the cracking of crude oil into refined products. In the latter case, isomorphs substation of Si to other metal atoms with high coordination number such as Titanium could produce the oxidation catalyst.[4] In both case, the characteristically microporous structure of zeolite catalysts endows the ''*shape-selective*'' effects on reactants, reaction transitions, and the products.[5]

- *Gas separation*. The gas separation performance of zeolite materials not only rely on their microporous structures directly, but also the affinity effects should also be taken into consideration. Typical examples including the CO_2/N_2, and CO_2/CH_4 separations.[6]

- *Ion-exchange*. Utilizing zeolite materials as detergents is the largest application segment. The loosely extra-framework cations could be exchanged readily which can be used to soften the water or remove the contaminative ions in water.[7]
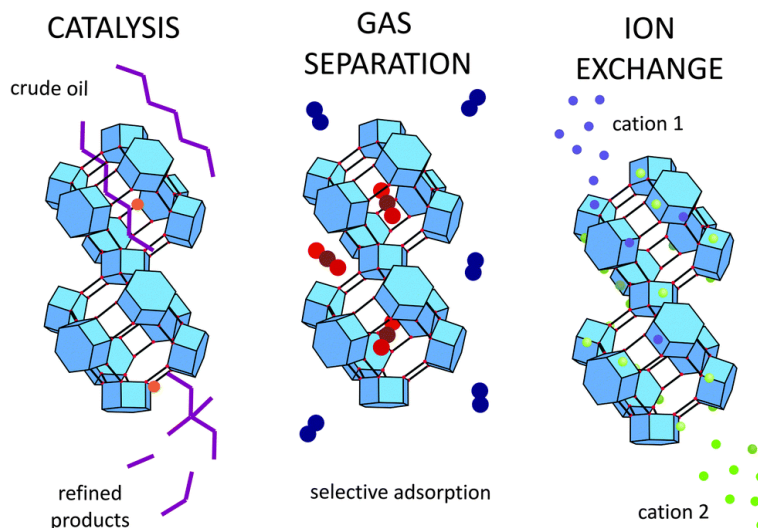
Figure 2 Main applications of zeolites.[2]

Particularly, due to the increased request on sustainable processes from both of energetic and environmental viewpoints,[8] zeolite catalysts have found new roles in refinery industry fields during which alternative biomass feedstock could be used instead of the crude oil. The extended utilization

of zeolite catalysts are also benefited from their intrinsic properties such as porous structures and acidity , while new challenges of developing zeolite materials in this new field cannot be ignored. For instance, as the feedstock shift from crude oil to biomass, the diffusion efficiency, pore connectivity, and hydrothermal stability of zeolite catalysts should be optimized as well (Figure 1.3).[9]
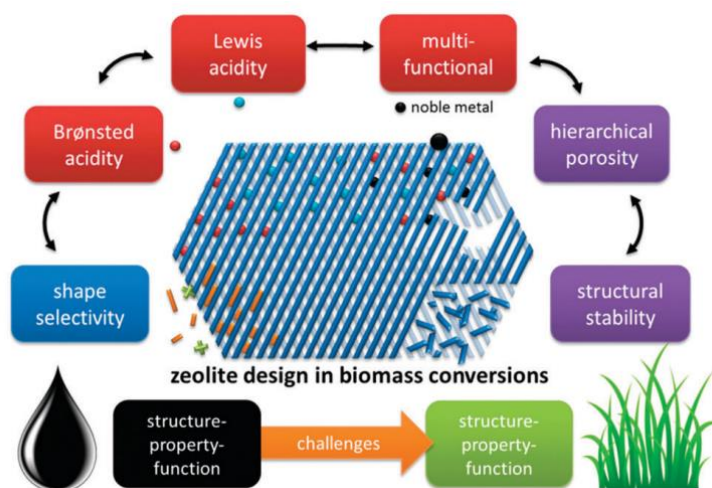
Figure 1.3 Concepts of zeolite catalysis in biomass conversion and petroleum-based processes.[9]

1.2 Hydrothermal synthesis of zeolites

Date back to 1940s, when Richard Barrer proposed an artificial synthesis route for zeolites using water as the solvent, the so-called "hydrothermal synthesis" have dominated the crystallization process from amorphous phase to zeolite crystal.[10] A typical reactants mixture for zeolite synthesis contains the Si source, Al source, mineralizers, organic structure-directing agents (OSDA), and water. After a well performed mixing and aging step, the so-called "gel" is obtained for further treatment under high temperatures (e.g. 100–200 ℃) for producing metastable zeolite phase (Figure 1.4). Besides the initial composition of gel, the crystallization process of zeolites can be affected by various parameters including the nature of the reactants, composition of the reaction mixture, mixing and aging procedures, seeding, nature of the reactor, crystallization temperature, pressure, agitation, and heating time.[11]
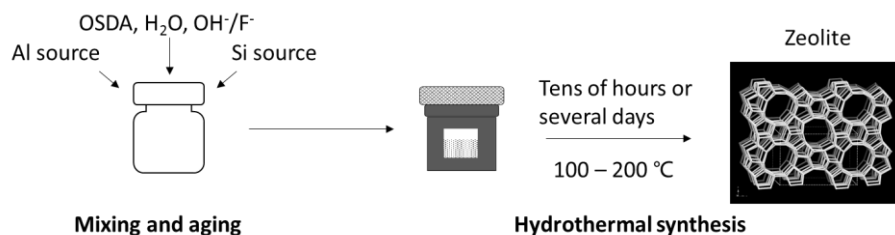
Figure 1.4 Illustration of hydrothermal synthesis of zeolites

Zeolite crystallization consists of two steps: nucleation and crystal growth. As the initial mixing process of reactants, the gel reaches a high supersaturate point where nuclei can form followed by the crystal growth until a hydrodynamic equilibrium between the zeolite formation and the solution. Considering the transformation from gel to zeolite crystal, two main synthesis mechanism were proposed as solution-mediated crystallization and *"in-situ"* rearrangement (Figure 1.5).[12] In the previous route (Figure 1.5a), under specific conditions, the solubility of the gel is high enough to adapt framework-forming species in solutions which further bound to crystals.[13-16] The dissolution of the gel lasts until the disappearance of the gel. After that, metastable and/or stable zeolites may crystallize based on the supersaturate degree. Whereas in the latter case (Figure 1.5b), it was proposed that the gel could *"in-situ"* transform into crystalline zeolites through a solid-solid reaction.[17-20] For either mechanism, corresponding evidence can be found which may alludes the diversity of the mechanism routes as the different hydrothermal synthesis conditions.
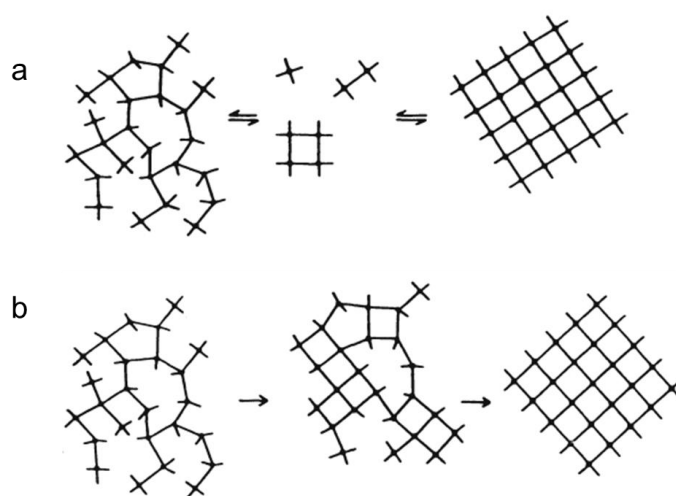
Figure 1.5 Schematic representation of solution-mediated crystallization (a) and "*in-situ*" rearrangement for zeolite formation (b).[12]

1.3 Ultrafast synthesis of zeolite

The natural zeolite can be formed under geological conditions for years. Despite of the much shortened artificial synthesis for zeolites, tens of hours or several days (in some cases, several weeks) are still needed, which presented as a substantial obstacle for industrial application of zeolite materials. There have been tremendous efforts to accelerate the hydrothermal synthesis of zeolite since considerable benefits on the energy and time cost can be expected. Typical examples including the microwave- and/or seed-assisted synthesis, inter-zeolite conversion (IZC) and radically faster synthesis.[20-24] The accelerating effects are generally realized by taking the crystallization pathway into consideration, for instance, enhancing interaction by overheating, skipping the induction period, and etc. In recent years, an ultrafast route for synthesizing zeolites by changing the reactors from conventional autoclaves to tubular reactors is developed to produce some industrially important zeolitic materials such as $AlPO_4$-5, SSZ-13, and ZSM-5 in just several minutes. A comprehensive summary about how this method works has been reviewed recently (Figure 1.6).[25]

Generally, the kinetically controlled induction period and the metastable zeolite phase are two significant problems hindering the fast crystallization of zeolite. For successfully developed ultrafast synthesis, synergistic effects among several factors were considered: aging and seeding effects, employment of high synthesis temperatures and the use of tubular reactor featuring fast heating.
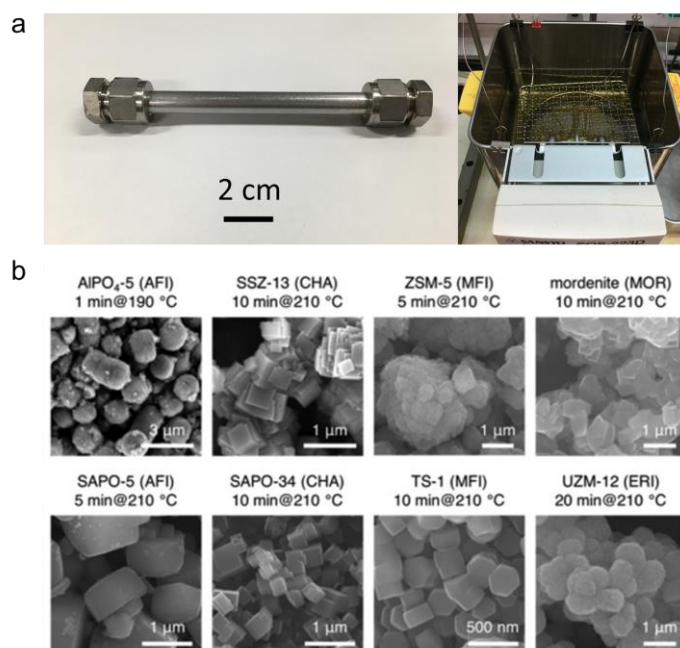
Figure 1.6 Ultrafast synthesis using tubular reactor and oil bath (a) for targeted zeolites (b). [25]

- *Aging.* Aging has long been recognized to be beneficial during hydrothermal synthesis. For ultrafast synthesis, the aging step offered a number of effects including i) making a homogenous mixture, ii) enhancing the interaction between inorganic and organic species, and iii) enhancing the interaction between seed and solution species.[26]

- *Seeding.* Nucleation is thought to be one of most critical kinetic barrier for fast crystallization. The addition of seed is useful to skip such kind of long period requested because a secondary nucleation could occur. Based on the existed seeding surface, not only undesired heterogeneous nucleation was suppressed but also a directing effect for desired zeolite phase was expected.[27]

- *High temperatures.* Compared with the nucleation, crystal growth is a kinetically faster step. Temperature is proved to be one of the most sensitive parameters than determine the crystal growth rate. With the assistance of aging and addition of seed, the crystal growth rate for targeted zeolite phase can be straightforwardly accelerated by increasing the synthesis temperature. For instance, under 210 ℃, the crystal growth rate of Silicalite-1 could be as fast as ca. 10^3–10^4 nm·h^{-1}, while under conventional synthesis of Silicalite-1, the speed was much slower as ca. 10 nm·h^{-1}.[28-30]

- *Fast heating.* Besides the employment of high temperature, special reactor featuring fast heating should also be noted. In conventional autoclaves, the temperature increase and down step could cost ca. 2 hours to reach a balanced heat transfer while for a home-made stainless tubular reactor, high temperature as 210 ℃ takes only 1 minute to activate the fast crystallization.[31]

Combined all these aforementioned favorable parameters, ultrafast synthesis achieved in several minutes becomes possible. A generalized pathway for displaying these affecting parameter during ultrafast synthesis is shown Figure. 1.7.[26]
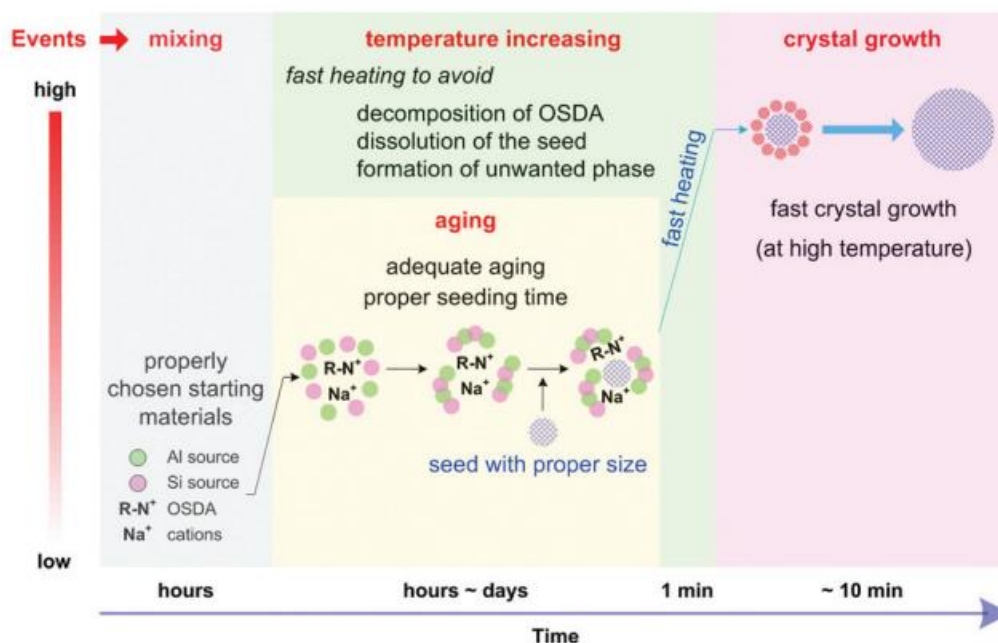
Figure 1.7 A generalized scheme for ultrafast synthesis, in which, the occurred events was differentiated at time stages.[26]

Despite the considerable progresses on ultrafast synthesis for a series of industrially important zeolite materials, the potential of this strategy is far from being fully revealed. By using tubular reactor featuring fast heating under high temperatures, a precisely controllable hydrothermal treatment could be anticipated. Resulting from which, there are several fields in which ultrafast synthesis strategy could be applied: i) continuously adjustable properties such as crystal size, morphologies, acidities and so on; ii) selective synthesis of zeolite phase which is difficult to be obtained in a pure form; iii) orientated, highly efficient post-synthesis for desirable properties.

1.4 The role of post-synthesis modifications

Zeolite materials can be used in diversified applications due to their adjustable properties. Therefore, introducing desired properties in zeolite materials is highly important to fulfill the increased requests from extended applications. As mentioned in above parts, hydrothermal synthesis of zeolites can be affected by various parameters, which makes the direct synthesis a primary way for controlling the properties of zeolite products. For instance, the Si/Al can be facilely controlled by the initial reaction composites while on the other hand the mesopores could be easily introduced into

zeolite by adding hard-templates at the initial synthesis stage.[32] Additionally, by changing the initial reaction composition such as introducing some heteroatoms like Ge, new zeolite structures are possibly obtained.[33] In addition to the direct synthesis, post-synthesis treatments to tailor zeolite properties have been and will continue to be indispensable to address the different requests from practical applications, especially regarding the large-scale preparation as well as low cost.[34] Starting from the routine drying and template removal processes that every zeolite must experience prior to use, a wide spectrum of treatments exists to alter individual or collective characteristics of these materials for optimal performance.

Table 1.1 Overview of commonly used post-synthesis modifications on zeolites[35]

Level	Method	Goal	Treatment
Micropore	Thermal activation	Dehydration, template removal	• Calcination in different atmosphere
	Chemical activation	Template removal	• Oxidative (H_2O_2, O_3, UV) • Dielectric-barrier discharge plasma
	Functionalization	Hybrid material production, pore and surface modification, passivation of unselective sites	• Immobilization of organics • Covalent/electrostatic grafting • Chemical liquid deposition
	Metal deposition and incorporation	Creation of active sites (reduction, sintering), control of pore openings, passivation of unselective sites	• Ion exchange • Chemical vapor deposition • Impregnation • Ion beam implantation
Framework	Isomorphs substitution	Acidity modification	• Hydrothermal, gas phase
	Demetallation	Composition, acidity, and stability modification	• Steaming • Acid/base leaching • H_2O_2 and microwave irradiation
	Secondary synthesis	Framework conversion, composite materials formation	• Hydrothermal • Steam assisted
Crystal/ particle	Demetallation	Introduction of secondary porosity	• Steaming • Acid/base leaching • H_2O_2 and microwave irradiation
	Tribochemical treatment	Size modification	• Milling
	Morphological constructions	Crystal/particle organization	• Aggregation • Pillaring • Delamination • Secondary growth

Particularly, for zeolite catalysts, the goal of post-synthesis treatments is to optimize their catalytic performance by increasing the favorable characteristics and/or decreasing the unfavorable ones. The typical post-synthesis treatments can be classified into i) atomic level (*e.g.* introduction or substitution of hetero- T-atoms), ii) microporous level (*e.g.* surface functionalization by organic or inorganic species), and iii) crystal and particle levels (*e.g.* introduction of secondary porosity).[35] Table 1.1 showed the most common post-synthesis treatments and the resultant effects on zeolite properties. With these post-synthesis treatments, the intrinsic properties of zeolites such as pore accessibility, active sites distribution, hydrothermal and thermal stability, crystal size, and crystal shape can be controlled in facile and economical ways.

In past decade, the number of zeolitic framework keeps increasing continuously. Moreover, besides the classical zeolites having pore sizes of 0.3–0.8 nm, developments of germanosilicate with extra-large pores (1–2 nm)[36] or other zeolite-type materials such as MOFs (Metal organic frameworks)[37-39] and ZIFs (Zeolite imidazolate frameworks)[40-42] further bridge up the gap between microporous materials and mesoporous materials (>2 nm). Despite the enrichment of porous materials benefited from the artificial synthesis strategy, the industrial application of newly discovered microporous materials is very rare. Till now, most of the industrial applications of zeolite materials are still based on the dawn of the zeolite commercialization, that is, only six structures, namely FAU-, MOR-, MFI-, FER-, LTA- and BEA type, cover more than 90% of all the applications.[35] The limited utilization of other zeolite structures is due to the stringent requirements from industrial viewpoint that not only the particularly intrinsic property is desired but also the weight of economic, environmental, and production issues take the equal importance before the final decision. Among the critical factors determining a zeolite type to practical applications, whether the zeolite can undergo a sustainable and efficient post-synthesis modifications is a crucial aspect.

For instance, preparation of core-shell structured zeolite is an effective way to utilize the properties of both zeolite core and zeolite shell simultaneously for high performance zeolite materials. A typical example of core-shell structured ZSM-5@Silicalite-1 showed much enhanced production selectivity of para-xylene during the alkylation of toluene. However, such kind of secondary growth of Silicalite-1 shell on the ZSM-5 core usually takes considerably long periods under batched operation conditions. This similar problem of low-efficient preparation for other core-shell structured zeolite materials, as confirmed in currently reported studies (Figure 1.8), hindered the practical

applications of this kind of highly functional materials.
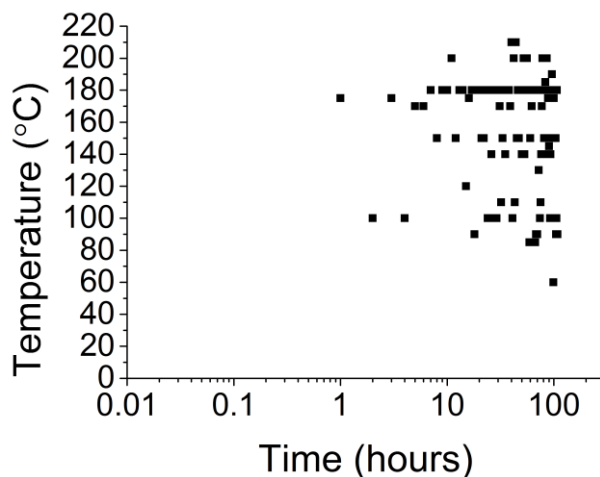
Figure 1.8 Current studies regarding preparation of core-shell structured zeolites through secondary growth. (Summarized from data base "web of science" by searching keywords of "zeolite" AND "Secondary growth" OR "Core-shell")

1.5 Continuous flow chemistry

Continuous flow chemistry is defined as the chemical processes proceeded in a continuously flowing stream rather than in the batched production.[43] Generally, microfluidic reactors made from non-reactive materials such as stainless, polymers, glasses are powerful tools to enable such kind of flow reactions. Over the years, there have growing applications of continuous flow technology regarding the processes involving special chemicals (photochemistry, electrochemistry, industrial gases, catalysts, ionic liquids, and etc.)[44-48] and pharmaceuticals (diagnostics, vitamins, and etc.)[49-50] in both academia and industrial area. The advantages of continuous flow process over the conventional batched reactions include the superior reproducibility, controlled reactions and being automatable. Moreover, the high surface area to volume ratio of the microfluidic reactor guarantees the uniform and rapid mixing process as well as a much enhanced heating transfer efficiency. A comprehensive comparison between the batched operation and continuous flow process is shown in Table 2.[51]

In recent years, besides the organic molecules, several examples of preparing nanoparticles through continuous flow system are also demonstrated, for instance, the CdSe quantum dots, platinum, silver, gold, rhodium nanoparticles and so on.[52-56] These successful examples indicate the high

potential of producing functional nanoparticles through an easily saleable way, *i.e.* the continuous flow preparation.

Table 1.2 Comparison of batch and continuous process operation for small-scale production[51]

Criterion	Batch process		Continuous process	
Product quality	−	variable	+	Constant
Optimal product quantities	−	small: on demand	+	medium/large in store
Process flexibility	+	high, multi-purpose plants	−	limited
Automatization	−	complex	+	straightforward
Labor costs	−	high	+	low
Process control needs	−	high	+	low
Set-up times	−	long	+	minimal
Cleaning	−	laborious	+	in design
Start-up and shutdown		not applicable	−	complex
Long reaction times	+	possible	−	difficult
Investment	+	low	−	high
Maintenance/Troubleshooting	+	common equipment	−	difficult "one of a kind

Generally, it was thought difficult to applied the flow chemistry to zeolite synthesis due to the much longer periods of zeolite synthesis (hours and days scale) than the common residence periods during continuous flow chemistry (seconds and minutes scale). Benefited from the above discussed ultrafast synthesis of zeolites in several minutes, the continuous production of zeolites becomes possible since 2014.[57] A typical establishment of continuous flow for ZSM-5 zeolite is shown in Figure 1.9.[58] Despite several successful cases of synthesizing zeolites in a continuous way, how to efficiently producing the functional zeolite materials with favorable properties related to practical applications is still an important issues to be studied, for instance, the porosity and acidity.
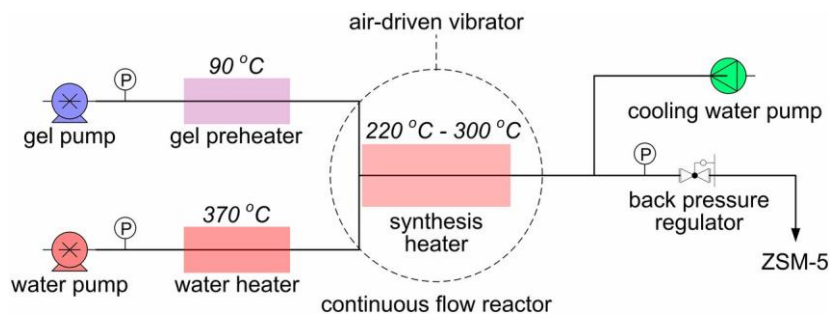
Figure 1.9 Illustrated continuous flow synthesis of ZSM-5.[58]

1.6 Objective and overview of this doctoral thesis

Inspired by the aforementioned background, developing an efficient way for function zeolite materials with desired properties is highly desired for promoting practical applications of zeolite materials. The traditional processes of introducing desired properties into zeolites often take disadvantages of long-term treatments and/or less-controlled production. To address these disadvantages, the objective of this doctoral thesis is to achieve ultrafast and controllable preparation functional zeolite materials with desired properties in extremely short periods, which could further allow the establishment of continuous flow chemistry for industrial production.

Introducing desired properties in zeolites can be achieved in either direct-synthesis or post-synthesis way. There have been some case studies for synthesizing zeolites in several minutes as discussed in previous parts, and the favorable influences of high temperatures and fast heating have been proved for shortening the hydrothermal crystallization step. Nevertheless, the investigation on accelerating post-synthesis modifications is very rare despite conditions similar to zeolite synthesis are often involved. The interaction between treating conditions and the parent materials has not been fully characterized, especially when the processes can possibly be finished in several minutes. One of the objectives of this thesis is to firstly investigate the possibility of synthesizing zeolites with desired properties through ultrafast strategy by considering the distinguished high temperature and shorted periods involved. (Figure 1.10) Further, for selected hydrothermal post-synthesis treatments, ultrafast approaches are to be established which is extremely interesting in both of i) practical viewpoint that open the new insight of facilitating industrial applications of more functional zeolite materials and ii) fundamental viewpoint that test the limitation of structural flexibility of crystalline zeolites toward external stimulus (Figure 1.10).

12
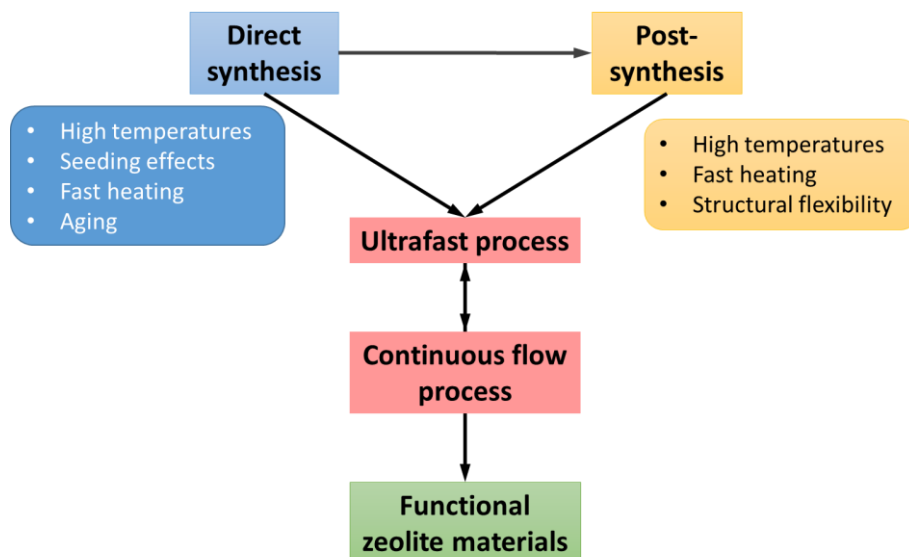
Figure 1.10 Objective and strategies of this thesis
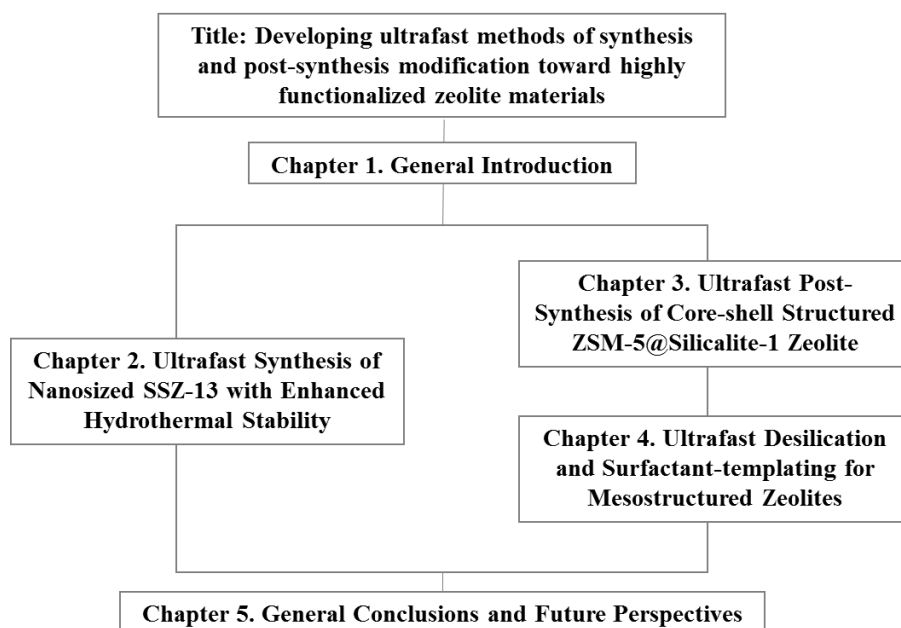
Figure 1.11 Structure of this doctoral thesis

To be more specific, firstly, for a direct ultrafast synthesis, the possible beneficial influence of high temperatures and the precisely controllable timing programs initiated the targeted preparation of nanosized zeolites with superior properties such as hydrothermal stability. On the other hand, as the acidity distribution and inter-connected porosity are two characteristic features for zeolite catalysts which relate to their catalytic performance including selectivity, diffusion efficiency, and catalyst life, post-synthesis for introducing such kind of favorable properties in zeolites were fully investigated.

The crystalline zeolites proved to take ultra-high structural flexibility which allowed them to accommodate the change of properties in short as several minutes by post-synthesis treatments.

The structure of this thesis is shown in Figure 1.11. Chapter 1 describes a general introduction on the background and motivation of this study. In Chapter 2, ultrafast synthesis of nanosized SSZ-13 zeolite with excellent hydrothermal stability is presented. A two-stage treatment using low temperature (low-T) and high temperature (high-T) was applied for that achievement. Comparative studies by adjusting the temperature programs revealed a possible pathway from which nanosized zeolite with superior properties could be obtained. Compared with the direct synthesis resulting in zeolites with favorable properties, in Chapter 3, a selected post-synthesis treatment, namely secondary crystal growth was further investigated to control the surface acidity of zeolite materials. By illuminating the fact that additional zeolite structures can formed on an existed external surface in very short periods, a possibly fast coating technology is proposed to fulfill various requests on surface modification. Besides the ultrafast surface modification, interactions between liquid reagents with zeolite inside structures are disclosed in Chapter 4. Zeolite materials behaved surprisingly high structural flexibility which allowed them to accommodate the ultrafast changed porous properties. All these ultrafast direct-synthesis and post-synthesis treatments aiming at zeolites with increased functional properties had opened a new insight on extending more zeolite structures into industrialization by developing efficient modifications. Then, general conclusions and future perspective are given in Chapter 5, followed by Acknowledgement which finally closes this thesis.

Reference

[1]   X. Qinhua, Y. Aizhen, Hydrothermal synthesis and crystallization of zeolites, *Prog. Cryst. Growth & Charact.* **1991**, 21, 29-70.

[2]   V. Van Speybroeck, K. Hemelsoet, L. Joos, M. Waroquier, R.G. Bell, C.R.A. Catlow, Advances in theory and their application within the field of zeolite chemistry, *Chem. Soc. Rev.* **2015**, 44, 7044-7111.

[3]   W. Vermeiren, J.-P. Gilson, Impact of zeolites on the petroleum and petrochemical industry, *Top. Catal.* **2009**, 52, 1131-1161.

[4]   M.A. Camblor, M. Costantini, A. Corma, L. Gilbert, P. Esteve, A. Mart ńez, S. Valencia, Synthesis and catalytic activity of aluminium-free zeolite Ti-β oxidation catalysts, *Chem. Commun.* **1996**, 1339-1340.

[5]   L. Rollmann, D. Walsh, Shape selectivity and carbon formation in zeolites, *J. Catal.* **1979**, 56.

[6]   B. Liu, B. Smit, Comparative molecular simulation study of CO2/N2 and CH4/N2 separation in zeolites and metal− organic frameworks, *Langmuir* **2009**, 25, 5918-5926.

[7]   L. Ćurković, Š. Cerjan-Stefanović, T. Filipan, Metal ion exchange by natural and modified zeolites, *Water Res.* **1997**, 31, 1379-1382.

[8]   Y. Li, L. Li, J. Yu, Applications of zeolites in sustainable chemistry, *Chem* **2017**, 3, 928-949.

[9]   T. Ennaert, J. Van Aelst, J. Dijkmans, R. De Clercq, W. Schutyser, M. Dusselier, D. Verboekend, B.F. Sels, Potential and challenges of zeolite chemistry in the catalytic conversion of biomass, *Chem. Soc. Rev.* **2016**, 45, 584-611.

[10]   C.S. Cundy, P.A. Cox, The hydrothermal synthesis of zeolites: history and development from the earliest days to the present time, *Chem. Rev.* **2003**, 103, 663-702.

[11]   C.S. Cundy, P.A. Cox, The hydrothermal synthesis of zeolites: Precursors, intermediates and reaction mechanism, *Micropor. Mesopor. Mater.* **2005**, 82, 1-78.

[12]   J.-L. Guth, H. Kessler, Synthesis of aluminosilicate zeolites and related silica-based materials, Catalysis and Zeolites, Springer1999, pp. 1-52.

[13]   S. Mintova, N.H. Olson, V. Valtchev, T. Bein, Mechanism of zeolite A nanocrystal growth from colloids at room temperature, *Science* **1999**, 283, 958-960.

[14]   S. Mintova, N.H. Olson, T. Bein, Electron microscopy reveals the nucleation mechanism of

zeolite Y from precursor colloids, *Angew. Chem. Int. Ed.* **1999**, 38, 3201-3204.

[15] B. Schoeman, J. Sterte, J.-E. Otterstedt, Analysis of the crystal growth mechanism of TPA-silicalite-1, *Zeolites* **1994**, 14, 568-575.

[16] J. Weitkamp, L. Puppe, Catalysis and zeolites: fundamentals and applications, Springer Science & Business Media 2013.

[17] R. Van Grieken, J. Sotelo, J. Menendez, J. Melero, Anomalous crystallization mechanism in the synthesis of nanocrystalline ZSM-5, *Micropor. Mesopor. Mater.* **2000**, 39, 135-147.

[18] D. Serrano, R. Van Grieken, P. Sanchez, R. Sanz, L. Rodrıguez, Crystallization mechanism of all-silica zeolite beta in fluoride medium, *Micropor. Mesopor. Mater.* **2001**, 46, 35-46.

[19] D. Serrano, M. Uguina, G. Ovejero, R. Van Grieken, M. Camacho, Evidence of solid-solid transformations during the TS-1 crystallization from amorphous wetness impregnated SiO2 TiO2 xerogels, *Micropor. Mater.* **1996**, 7, 309-321.

[20] C. Cundy, J. Zhao, Remarkable synergy between microwave heating and the addition of seed crystals in zeolite synthesis—a suggestion verified, *Chem. Commun.* **1998**, 1465-1466.

[21] K. Iyoki, K. Itabashi, T. Okubo, Progress in seed-assisted synthesis of zeolites without using organic structure-directing agents, *Micropor. Mesopor. Mater.* **2014**, 189, 22-30.

[22] S. Goel, S.I. Zones, E. Iglesia, Synthesis of zeolites via interzeolite transformations without organic structure-directing agents, *Chem. Mater.* **2015**, 27, 2056-2066.

[23] L. Van Tendeloo, E. Gobechiya, E. Breynaert, J.A. Martens, C.E. Kirschhock, Alkaline cations directing the transformation of FAU zeolites into five different framework types, *Chem. Commun.* **2013**, 49, 11737-11739.

[24] G. Feng, P. Cheng, W. Yan, M. Boronat, X. Li, J.-H. Su, J. Wang, Y. Li, A. Corma, R. Xu, Accelerated crystallization of zeolites via hydroxyl free radicals, *Science* **2016**, 351, 1188-1191.

[25] Z. Liu, J. Zhu, T. Wakihara, T. Okubo, Ultrafast synthesis of zeolites: breakthrough, progress and perspective, *Inorg. Chem. Front.* **2019**, 6, 14-31.

[26] M. Ogura, Y. Kawazu, H. Takahashi, T. Okubo, Aluminosilicate species in the hydrogel phase formed during the aging process for the crystallization of FAU zeolite, *Chem. Mater.* **2003**, 15, 2661-2667.

[27] Y. Kamimura, S. Tanahashi, K. Itabashi, A. Sugawara, T. Wakihara, A. Shimojima, T. Okubo,

Crystallization behavior of zeolite beta in OSDA-free, seed-assisted synthesis, *J. Phys. Chem. C* **2010**, 115, 744-750.

[28]   A. Ghorbanpour, A. Gumidyala, L.C. Grabow, S.P. Crossley, J.D. Rimer, Epitaxial growth of ZSM-5@Silicalite-1: A core–shell zeolite designed with passivated surface acidity, *ACS nano* **2015**, 9, 4006-4016.

[29]   J. Hedlund, S. Mintova, J. Sterte, Controlling the preferred orientation in silicalite-1 films synthesized by seeding, *Micropor. Mesopor. Mater.* **1999**, 28, 185-194.

[30]   C. Peng, Z. Liu, Y. Yonezawa, Y. Yanaba, N. Katada, I. Murayama, S. Segoshi, T. Okubo, T. Wakihara, Ultrafast post-synthesis treatment to prepare ZSM-5@ Silicalite-1 as a core-shell structured zeolite catalyst, *Micropor. Mesopor. Mater.* **2019**, 277, 197-202.

[31]   Z. Liu, T. Wakihara, C. Anand, S.H. Keoh, D. Nishioka, Y. Hotta, T. Matsuo, T. Takewaki, T. Okubo, Ultrafast synthesis of silicalite-1 using a tubular reactor with a feature of rapid heating, *Micropor. Mesopor. Mater.* **2016**, 223, 140-144.

[32]   W. Fan, M.A. Snyder, S. Kumar, P.-S. Lee, W.C. Yoo, A.V. McCormick, R.L. Penn, A. Stein, M. Tsapatsis, Hierarchical nanofabrication of microporous crystals with ordered mesoporosity, *Nat. Mater.* **2008**, 7, 984.

[33]   Q. Li, A. Navrotsky, F. Rey, A. Corma, Enthalpies of formation of Ge-zeolites: ITQ-21 and ITQ-22, *Micropor. Mesopor. Mater.* **2004**, 74, 87-92.

[34]   C.Y. Chen, S.I. Zones, Post‐Synthetic Treatment and Modification of Zeolites, *Zeolites and Catalysis: Synthesis, Reactions and Applications* **2010**, 155-170.

[35]   V. Valtchev, G. Majano, S. Mintova, J. Pérez-Ramírez, Tailored crystalline microporous materials by post-synthesis modification, *Chem. Soc. Rev.* **2013**, 42, 263-290.

[36]   J. Jiang, J. Yu, A. Corma, Extra–large–pore zeolites: bridging the gap between micro and mesoporous structures, *Angew. Chem. Int. Ed.* **2010**, 49, 3120-3145.

[37]   J. Lee, O.K. Farha, J. Roberts, K.A. Scheidt, S.T. Nguyen, J.T. Hupp, Metal–organic framework materials as catalysts, *Chem. Soc. Rev.* **2009**, 38, 1450-1459.

[38]   J.-R. Li, R.J. Kuppler, H.-C. Zhou, Selective gas adsorption and separation in metal–organic frameworks, *Chem. Soc. Rev.* **2009**, 38, 1477-1504.

[39]   H. Li, M. Eddaoudi, M. O'Keeffe, O.M. Yaghi, Design and synthesis of an exceptionally stable and highly porous metal-organic framework, *Nature* **1999**, 402, 276.

[40] K.S. Park, Z. Ni, A.P. Côté, J.Y. Choi, R. Huang, F.J. Uribe-Romo, H.K. Chae, M. O'Keeffe, O.M. Yaghi, Exceptional chemical and thermal stability of zeolitic imidazolate frameworks, *Proc. Natl. Acad. Sci. U.S.A.* **2006**, 103, 10186-10191.

[41] R. Banerjee, A. Phan, B. Wang, C. Knobler, H. Furukawa, M. O'keeffe, O.M. Yaghi, High-throughput synthesis of zeolitic imidazolate frameworks and application to CO2 capture, *Science* **2008**, 319, 939-943.

[42] A. Phan, C.J. Doonan, F.J. Uribe-Romo, C.B. Knobler, M. O'keeffe, O.M. Yaghi, Synthesis, structure, and carbon dioxide capture properties of zeolitic imidazolate frameworks, *Acc. Chem. Res* **2010**, 43, 58-67.

[43] F.M. Akwi, P. Watts, Continuous flow chemistry: where are we now? Recent applications, challenges and limitations, *Chem. Commun.* **2018**, 54, 13894-13928.

[44] D. Cambie, C. Bottecchia, N.J. Straathof, V. Hessel, T. Noel, Applications of continuous-flow photochemistry in organic synthesis, material science, and water treatment, *Chem. Rev.* **2016**, 116, 10276-10341.

[45] M.A. Kabeshov, B. Musio, P.R. Murray, D.L. Browne, S.V. Ley, Expedient preparation of nazlinine and a small library of indole alkaloids using flow electrochemistry as an enabling technology, *Org. Lett.* **2014**, 16, 4618-4621.

[46] F. Lévesque, P.H. Seeberger, Highly efficient continuous flow reactions using singlet oxygen as a "green" reagent, *Org. Lett.* **2011**, 13, 5008-5011.

[47] A. Kirschning, W. Solodenko, K. Mennecke, Combining enabling techniques in organic synthesis: continuous flow processes with heterogenized catalysts, *Chem. Eur. J.* **2006**, 12, 5972-5990.

[48] P.B. Webb, M.F. Sellin, T.E. Kunene, S. Williamson, A.M. Slawin, D.J. Cole-Hamilton, Continuous flow hydroformylation of alkenes in supercritical fluid−ionic liquid biphasic systems, *J. Am. Chem. Soc.* **2003**, 125, 15577-15588.

[49] B. Gutmann, D. Cantillo, C.O. Kappe, Continuous‐flow technology—a tool for the safe manufacturing of active pharmaceutical ingredients, *Angew. Chem. Int. Ed.* **2015**, 54, 6688-6728.

[50] L. Malet-Sanz, F. Susanne, Continuous flow synthesis. A pharma perspective, *J. Med. Chem.* **2012**, 55, 4062-4098.

[51]   A. Pashkova, L. Greiner, Towards Small‐Scale Continuous Chemical Production: Technology Gaps and Challenges, *Chem. Ing. Tech.* **2011**, 83, 1337-1342.

[52]   B.K. Yen, N.E. Stott, K.F. Jensen, M.G. Bawendi, A continuous−flow microcapillary reactor for the preparation of a size series of CdSe nanocrystals, *Adv. Mater.* **2003**, 15, 1858-1862.

[53]   C.T. Riche, E.J. Roberts, M. Gupta, R.L. Brutchey, N. Malmstadt, Flow invariant droplet formation for stable parallel microreactors, *Nat. Commun.* **2016**, 7, 10780.

[54]   X.Z. Lin, A.D. Terepka, H. Yang, Synthesis of silver nanoparticles in a continuous flow tubular microreactor, *Nano Lett.* **2004**, 4, 2227-2232.

[55]   J. Boleininger, A. Kurz, V. Reuss, C. Sönnichsen, Microfluidic continuous flow synthesis of rod-shaped gold and silver nanocrystals, *Phys. Chem. Chem. Phys.* **2006**, 8, 3824-3827.

[56]   P. Kunal, E.J. Roberts, C.T. Riche, K. Jarvis, N. Malmstadt, R.L. Brutchey, S.M. Humphrey, Continuous Flow Synthesis of Rh and RhAg Alloy Nanoparticle Catalysts Enables Scalable Production and Improved Morphological Control, *Chem. Mater.* **2017**, 29, 4341-4350.

[57]   Z. Liu, T. Wakihara, D. Nishioka, K. Oshima, T. Takewaki, T. Okubo, Ultrafast continuous-flow synthesis of crystalline microporous aluminophosphate $AlPO_4$-5, *Chem. Mater.* **2014**, 26, 2327-2331.

[58]   Z. Liu, K. Okabe, C. Anand, Y. Yonezawa, J. Zhu, H. Yamada, A. Endo, Y. Yanaba, T. Yoshikawa, K. Ohara, T. Okubo, T. Wakihara, Continuous flow synthesis of ZSM-5 zeolite on the order of seconds, *Proc. Natl. Acad. Sci. U.S.A.* **2016**, 113, 14267-14271.

Chapter 2 Ultrafast Synthesis of Nanosized SSZ-13 with Enhanced Hydrothermal Stability

2.1 Introduction

Zeolites are excellent shape-selective catalysts due to its unique microporous structures; however, the mass transfer efficiency from and to the active sites inside zeolites is also restricted considerably. Nanosized zeolites with relative shorter diffusion pathways showed superiority in catalytic efficiency as well as catalysts life compared with their micronsized counterparts.[1]

The methods to prepare nanosized zeolites can be classified into bottom-up and top-down routes. In the bottom-up ones, the crystal size is mainly manipulated by controlling kinetic behaviors in the nucleation and the crystal growth stages. Homogeneous mixture of silicate and aluminate species under low temperature breeds single nuclei which further grows into nanocrystal.[2] While when OSDAs are involved in the syntheses conditions, the rationally designed OSDAs can result in formation of three dimensional nanocrystals or two dimensional nanosheets.[3-6] Addition of growth modifiers or imposing micro-emulsion methodology can also yield nanosized zeolites.[7-8] A top–down approach recently developed by T. Wakihara *et al.* is mild bead milling followed by recrystallization. Through this route, a series of industrially important zeolites, including MFI, CHA, LTA, and AFX, have been successfully prepared with crystal size smaller than 100 nm.[9-12]

Nevertheless, the nanosized zeolites are usually recognized to have relatively poorer hydrothermal stability due to their large surface areas compared with their micronsized counter parts. Modifying the external surface with functional groups are effective ways to enhance the hydrothermal stability of zeolites, for instance, the deposition of silica layer or functionally connected with metal oxides.[13-14] However, these approaches take additional treatment which make the preparation process complicated and also could result in the decrease of the acid sites amount or blockage of the surface pore openings. Thus, a more facile method that can intrinsically help stabilize structure of nanosized zeolite is highly desired.

Temperature is a crucial factor in determining kinetic process during zeolite synthesis. Consequently, under different synthesis temperatures, zeolite products vary their zeolitic phase as

well as their morphologies.[15-16] A long-term hydrothermal synthesis under mild temperature is commonly expected to be favorable for synthesizing nanosized zeolites.[1] Not only the comprehensive induction period results in large amounts of nuclei formed, but also the steady treatment could suppress the Ostwald ripening effect that the growth of nanocrystals to larger ones can be hindered. On the other hand, the higher synthesis temperature has been found to be effective in improving the thermal stability of zeolites recently.[17-18] Likewise, hydrothermal stability of zeolites is expected to be improved in the same way, *i.e.*, the preparation of zeolite under higher synthesis temperature. Based on above backgrounds, there are several aspects to be considered to synthesizing the nanosized zeolites with high hydrothermal stability: i) controlled nucleation stage; ii) high temperature treatment; iii) fast process under high temperature.

The SSZ-13 zeolite with CHA topology has gained significant attention in recent years because of its excellent catalytic performance in the ammonia selectively catalytic reduction (NH_3-SCR) and methanol-to-olefins (MTO) reactions.[19-21] In particular, considering the highly humid atmosphere and high temperature at automobile engine where the catalysts work, preparing CHA zeolite with sufficient hydrothermal stability will be quite profitable. On the other hand, nanosized SSZ-13 zeolite has been prepared under conventional hydrothermal conditions costing several days, while its hydrothermal stability is not fully explored.[8, 22] There has been a research in which SSZ-13 zeolite could be obtained in 10 minutes through an ultrafast synthesis method, while the possible controlling effects on the crystal size has not been clarified.[23] Moreover, considering the high temperature employed in ultrafast synthesis compared with conventional one, it would extremely exciting to investigate how that kind of high temperature could affect the hydrothermal stability of zeolite products. Following this thought, nanosized zeolite with simultaneously controllable crystal size as well as excellent hydrothermal stability is expected. In this chapter, a two-stage temperature programed hydrothermal treatment, i.e. low-temperature and high-temperature, was applied to investigate the temperature effects in either stage on the properties of zeolite products. Mainly, the changes of crystal size and hydrothermal stability were taken into consideration. A compromised synthesis condition was finally selected for producing SSZ-13 zeolite having uniform nanosize and optimal hydrothermal stability. The main contents of this chapter has been published in reference 29.

2.2 Experiments

2.2.1 Materials and tools

The following chemicals were used as received without any further purification: Cab-O-Sil® (Grade M5, Cabot Co.), aluminum hydroxide $Al(OH)_3$ (Wako Pure Chemical Industries, Ltd.), and *N,N,N*-trimethyl-1-adamantanamine hydroxide (25 wt% TMAdaOH in H_2O, Mitsubishi Chemical Corporation). Deionized water was obtained from a Millipore water purification system. Silicone oil (KF968-1-100, Shin-Etsu Silicone) was used as a heating medium for the high-T process.

The tubular reactor was made from a standard stainless-steel tube (with an outer and an inner diameter (*o.d.* and *i.d.*) of 10 mm and 8 mm, respectively). The tube reactor was approximately 12.5 cm long and was sealed at both ends with stainless steel caps (SS-10MO-C, Swagelok). A bead milling apparatus (LMZ015, Ashizawa Finetech, Ltd., Tokyo, Japan) and an ultrasonic vibrator (VCX 600, Sonic & Materials Inc., USA) were used for the zeolite milling process. If no special notification, the tubular reactor used in other chapters is the same as described here. To avoid any duplication, the relative information will not be given twice.

2.2.2 Synthesis of raw SSZ-13 seed

Raw seed SSZ-13 zeolite was prepared with the reactant composition of 1 SiO_2: 0.025 Al_2O_3: 0.4 TMAdaOH: 16 H_2O using a conventional Teflon®-lined stainless-steel autoclave (#47499, Parr Instrument Company). First, the aluminum source was dissolved in TMAdaOH solution at 80 ℃ overnight. Water and silicon source were then added. 10 g of the mixed reactants were transferred into the autoclave and hydrothermally treated at 150 ℃ for 48 h. The product was recovered by centrifugation at 14,000 rpm for 5 min, thoroughly washed with water, and dried at 80 ℃ overnight. This sample was designated as raw seed.

2.2.3 Preparation of milled seed

The milled seed SSZ-13 was prepared on a bead milling apparatus fed with raw seed, following procedures reported previously.[9] Briefly, 15 g of raw seed SSZ-13 was dispersed in 330 mL of deionized water using an ultrasonic vibrator, and the slurry was fed by a gear pump into the milling chamber and pulverized for 60 min using zirconia beads of 300 μm in diameter. The agitation speed was set at 3,000 rpm. Thereafter, the milled slurry was collected and dried overnight at 80 ℃ to obtain milled SSZ-13. This sample was designated as milled seed.

2.2.4 Low temperature crystallization using raw and milled seed.

The reactant compositions were 1 SiO_2: 0.025 Al_2O_3: 0.4 TMAdaOH: 16 H_2O. SSZ-13 seed (10 wt%, raw or milled) on the basis of SiO_2 was then added. The mixed reactants were transferred into a 50 mL polypropylene bottle, and then hydrothermally treated for 0–240 hours at 95 °C. The products were recovered by centrifugation, washed thoroughly with deionized water, and dried at 80 °C overnight.

2.2.5 Two-stage synthesis of nanosized SSZ-13

After a prescribed period (x [h], 95 °C) of low-T treatment, the reactants were transferred into the tube reactor for further high-T (y [min], 210 °C) synthesis in a preheated oil bath. The products were then recovered by centrifugation, washed thoroughly with deionized water, and dried at 80 °C overnight. Samples prepared under different conditions were designated as x [h] + y [min]; for example, a 12 h + 20 min sample was treated for 12 h at low temperature, and then treated for 20 min at high temperature

2.2.6 Hydrothermal stability and catalytic reactions

Hydrothermal stability tests. As no alkali metal was used during syntheses, all of the as-calcined samples obtained after 10 h of calcination at 550 °C were protonated without further ion-exchange treatment, i.e., existed as H^+/SSZ-13. The H^+/SSZ-13 was used in the hydrothermal stability test. First, approximately 0.5 g of the calcined sample was heated to the desired temperature at 10 °C/min under dry air atmosphere with flow rate of 100 cm^3/min. After reaching the target temperature, humid air containing 10 vol% H_2O was introduced. Hydrothermal treatments lasted for 5 h at 700 °C, 750 °C, or 800 °C.

NH₃-SCR activity tests. The copper-exchanged SSZ-13 was preliminarily prepared by the following steps. The H^+/SSZ-13 was firstly added into 1 mol/L ammonium nitrate solution (0.3 g/10 mL) and then placed in an oven at 80 °C for 4 h. After washing and drying, the product obtained was then mixed with 3 wt% copper acetate solution (0.25 g/10 mL) followed by stirring at 70 °C for 15–30 min, depending on the particle size. After washing and drying, the powder was calcined at 550 °C for 3 h to obtain copper-exchanged SSZ-13 zeolite. NH₃-SCR activity tests of the copper-exchanged SSZ-13 zeolites were performed on a fixed-bed reactor made of quartz glass. The feed gas containing

350 ppm NO_x, 385 ppm NH_3, 15% O_2, 5% H_2O, and balanced N_2 was introduced at a constant speed of 200,000 h^{-1} (hourly space velocity). The effluent gas was analyzed using an online Thermo Nicolet NEXUS 670-FTIR spectrometer equipped with a heated multiple-path gas cell (2 m). The NO_x conversion was calculated as described in a previous report (Equation 1).[24] Hydrothermal aging was performed in a flow reactor at 800 ℃ for 5 h in air containing 10 vol% H_2O.

$$NO_x = \frac{(NO + NO_2)_{inlet} - (NO + NO_2 + N_2O)_{outlet}}{(NO + NO_2)_{inlet}} \times 100\% \qquad \text{(Equation 1)}$$

2.2.7 Characterizations

Powder X-ray diffraction (XRD) patterns of all the samples were obtained using Rigaku Ultima IV diffractometers with CuKα radiation (λ = 1.5406 Å, V = 40 kV, I = 40 mA) at a scanning rate of 4 ℃/min. The relative crystallinities of all samples were determined from the XRD patterns by calculating the areas under the peaks at 2θ = 20.8 °, 25.0 °, and 26.3 °, using raw seed as the standard at 100%. Morphologies of the products were observed using a field emission scanning electron microscope (FE-SEM, JSM-7000F, JEOL, Japan). Nitrogen adsorption–desorption measurements were performed on a Quantachrome Autosorb-iQ2 instrument at the temperature of liquid nitrogen with an outgas pretreatment at 400 ℃ for 6 h under vacuum. Elemental analysis was performed by a Thermo iCAP 6300 inductively coupled plasma−atomic emission spectrometer (ICP-AES). Aluminum–27 (^{27}Al) solid-state nuclear magnetic resonance (SSNMR) spectra of the samples were obtained on a JEOL ECA 800 (18.8 T) spectrometer at a Larmor frequency of 208.49 MHz. A JEOL 3.2 mm MAS probe was used for the measurements. Sample powders were packed in a 3.2 mm ZrO_2 rotor and spun at 20 kHz. The spectra were obtained by a single-pulse experiment with a short pulse (≤0.27 μs). Typically, 256 scans were collected for each sample and the pulse repetition time (1 s) was long enough to ensure full relaxation of the ^{27}Al spins. The ^{27}Al chemical shifts were calibrated with a 1M $Al(NO_3)_3$ aqueous solution as 0 ppm. Thermogravimetric and differential thermal analysis (TG-DTA) was conducted on a Rigaku PU 4K from 30 ℃ to 800 ℃ at a heating rate of 10 ℃/min under a flow of 10 vol% -O_2/90vol% -He mixed gas. High-energy X-ray total scattering (HEXTS) measurements were conducted at beamline BL04B2 of SPring-8, Japan. The powder sample was loaded in a quartz capillary and tested using a horizontal two-axis diffractometer. The incident X-ray energy was 61.4 keV (λ = 0.202 Å). The maximum Q collected in this study ($Q = 4\pi \sin\theta/\lambda$, where

θ and λ denote the scattering angle and photon wavelength, respectively), Q_{max}, was 25 Å^{-1}. The obtained data were analyzed by well-established procedures, including absorption, background, polarization, and Compton scattering corrections, followed by normalization to give the Faber−Ziman total structure factor $S(Q)$ [34–35]. The pair distribution function, $G(r)$, was then determined from $S(Q)$ by the following equation:

$$G(r) = 4\pi r[\rho(r) - \rho_0] = \frac{2}{\pi} \int_{Q_{min}}^{Q_{max}} Q[S(Q) - 1]\sin(Qr)dQ \quad \text{(Equation 2)}$$

where ρ_0 is the atomic number density (0.0435/Å^3, based on 15 Si: 1 Al: 32 O). To avoid any duplication, the same characterization methods used in other chapters will not be described again.

2.3 Results and discussions

2.3.1 Preparation of the seeds and their corresponding low-T synthesis behaviors
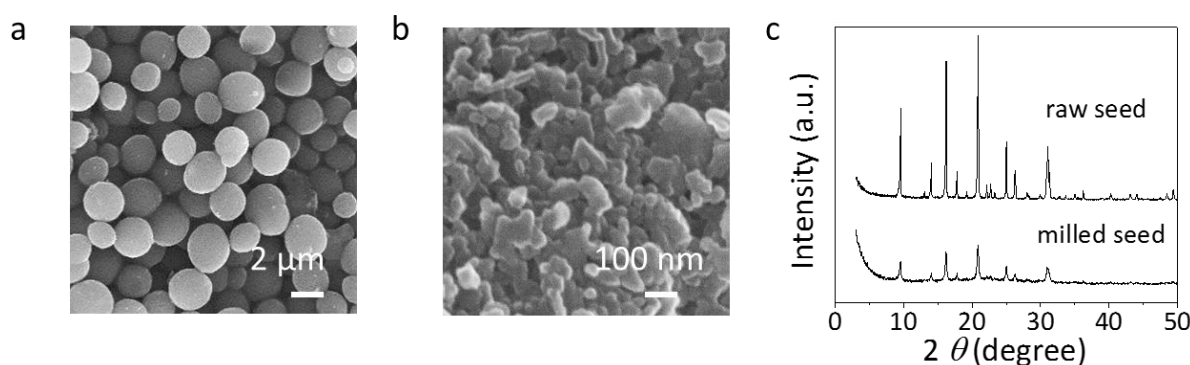
Figure 2.1 SEM images of synthesized raw SSZ-13 seed and milled seed (a, b), respectively. Corresponding XRD patterns (c), all the peaks belong to CHA topology.

The synthesized raw SSZ-13 seed shows a spherical morphology of 1−2 μm (Figure 1a), with strong XRD peaks which are assigned the CHA topology (Figure 1c). After the beads milling treatment which aimed at decreasing the seed size, the obtained milled seed takes anomalous shape with an approximate particle size of 50 nm (Figure 1b). Moreover, the XRD peaks of the milled seed shows remarkably decrease indicating the partially amorphization due to the physically interrupted crystalline structure (Figure 1c).
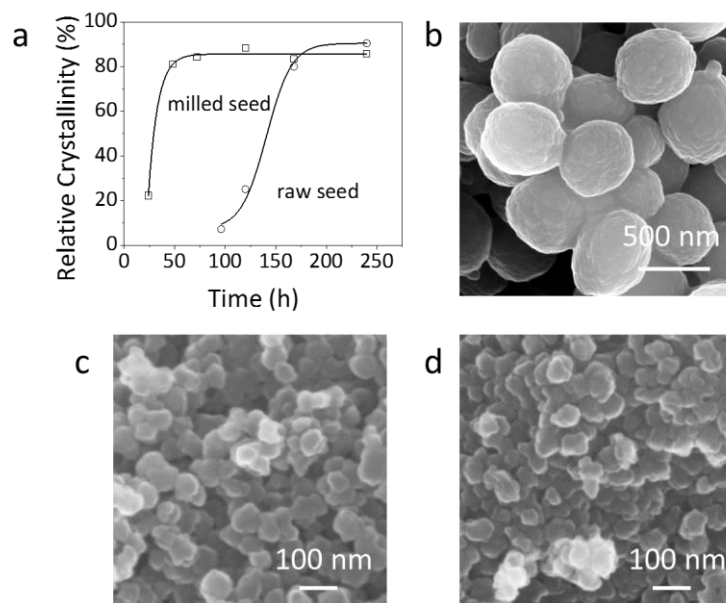
Figure 2.2 Crystallization curves of low-T synthesis (a) and SEM images of raw-240 h, milled-72 h, milled-168 h (b-d), respectively.

As previously reported, seed could help skip the relatively long induction period that synthesis period could be shortened considerably.[25] By using these two kinds of seed, syntheses of SSZ-13 zeolite were performed under a low-temperature condition (95 ℃). Generally, the synthesis of SSZ-13 zeolite is conducted under 140–160 ℃ without any seed, costing several days.[26] Herein, according to the crystal growth curves shown in Figure 2a, with the addition of seed, SSZ-13 zeolites are successfully obtained under relatively lower temperature, though considerably long periods are needed. The fully crystallizations for raw and milled seed condition occur at 240 h and 72 h, respectively. As seeds provide fundamental surfaces for further crystal growth, the larger surface areas of milled seed not only contributed to obvious reduction of induction period, but also allowed faster crystal growth intensively. Moreover, the resultant products also showed much different crystal size (Figure 2b and c). Under the raw seed condition, no crystal growth occurs until 96 h. In addition to the fact that crystal size of the product is smaller than that of raw seed (500 nm vs. 1–2 μm), a seed dissolution was suggested to have occurred at the initial stage. On the other hand, for the milled seed case, the crystal growth starts instantly and soon reaches its plateau. It is worth noting that, even the hydrothermal process was prolonged (*e.g.* 168 h), no significant change of crystal size was observed (Figure 2c and d), which indicated a suppressed Ostwald ripening effect under low temperatures. Thanks to the application of milled seed as well as low-temperature treatment, nanosized SSZ-13

having uniform size distribution around 50 nm was firstly obtained.

2.3.2 Disadvantages of nanosized SSZ-13 (milled-72 h) obtained under low-T synthesis

Although nanosized SSZ-13 was successfully obtained by low-T synthesis, the time required to reach full crystallization is still considerably long. Moreover, a non-negligible problem is that the nanosized zeolites obtained under low-T condition showed lower relative crystallinity (ca. 84%) as well as micropore volumes, which may imply the presence of structural defects compared with the raw seed. As described in the introduction part, the hydrothermal stability is a crucial factor catalytic performance of nanosized SSZ-13 zeolite. Hydrothermal stability tests at 700 ℃, 750 ℃, and 800 ℃ were conducted on raw SSZ-13 and milled-72 h. Changes of micropore volume and relative crystallinity are used to identify the effects on zeolite structure under different temperatures (Figure 2.3). After hydrothermal treatment at 800 ℃ for 5 h, the remaining crystallinity and micropore volume of raw SSZ-13 were about 60%. In contrast, the milled-72 h sample exhibits initially lower crystallinity and micropore volume followed by rapid decreases. These results suggested that the nanosized zeolite obtained under low-T condition cannot compete with the micronsized counterpart regarding the hydrothermal stability.
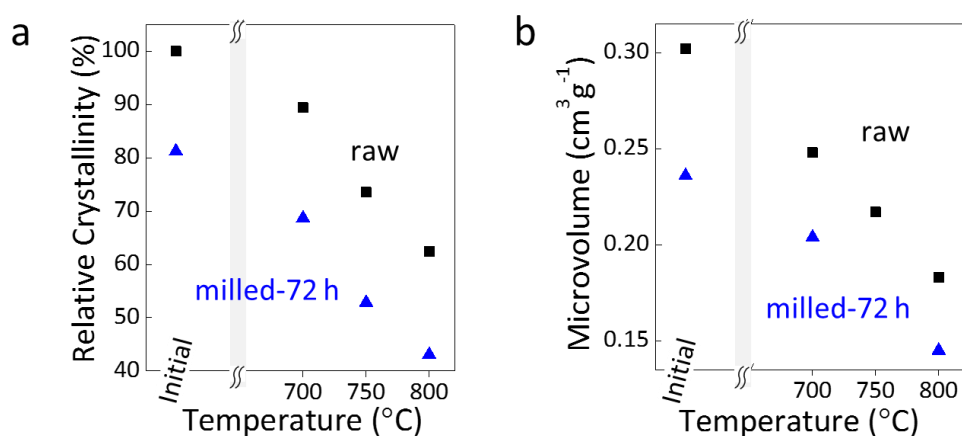
Figure 2.3 Changes of relative crystallinity (a) and micropore volumes (b) of raw and milled-72 h samples after hydrothermally treated under 700 ℃, 750 ℃, and 800 ℃ for 5 h in a humid air containing 10 vol% H_2O.

2.3.3 Preparation of nanosized SSZ-13 zeolite by a two-stage synthetic method
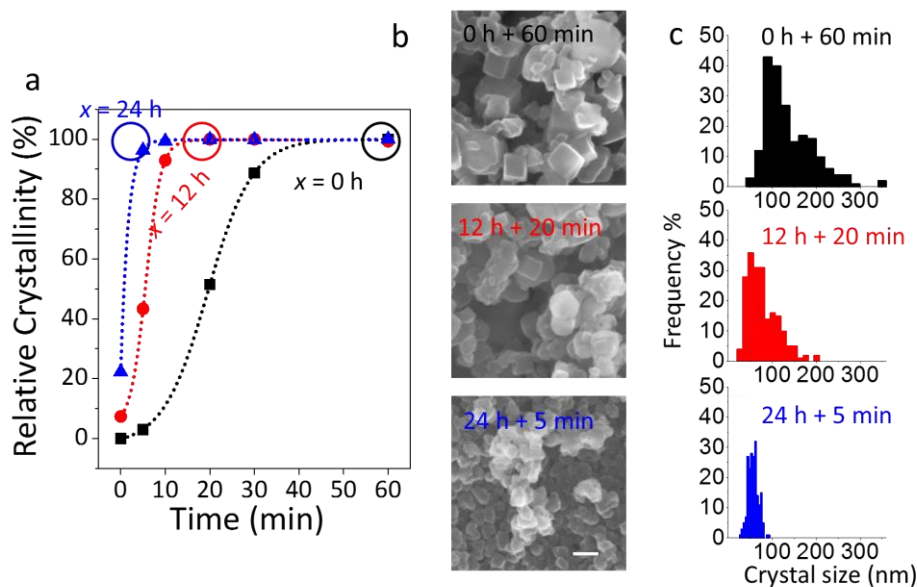
Figure 2.4 a, Crystallization curves of the high-T treatment after a low-T stage (x = 0–24 h, y = 0–60 min). b, SEM images high-T treated products, 0 h + 60 min, 12 h + 20 min, and 24 h + 5 min, respectively. c, particle size distributions of 0 h + 60 min, 12 h + 20 min, and 24 h + 5 min samples, calculation based on 200 particles in a single SEM image of each sample.

High synthesis temperature proves to be effective in accelerating the crystal growth as well as producing zeolites with stronger thermal stability. A two-stage synthesis treatment including sequential low-T synthesis and high-T synthesis was applied to address the aforementioned disadvantages of nanosized zeolites. Figure 2.4 presents the crystallization curves of samples under the low-T treatment (95 ℃, x h) followed by the high-T treatment (210 ℃, y min). As prolonged low-T treatment (namely, x h = 0, 12, and 24 h), the time for reaching full crystallization becomes shorter (namely, y min = 60, 20, 5 min). Three typical fully crystallized samples designated as "x h + y min" are 0 h + 60 min, 12 h + 20 min, 24 + 5 min, respectively. SEM images and corresponding crystal size distribution of these samples are shown in Figure 2.4b and c. The 0 h + 60 min sample shows a cubic morphology with a wide distribution (60–300 nm), which was due to the Ostwald ripening effects under high temperature. For 12 h + 20 min sample, the average crystal decreased to ca. 100 nm, and moreover, the crystal size distribution is narrowed. These results implied that the expected Ostwald ripening was suppressed even under the high-T treatment at 210 ℃. It is speculated that the uniform particle size distribution formed at low-T stage inhibited the further differentiation of crystal size during the ripening process, especially when the crystal growth period was shortened to the order

of minutes. A further extension of the low-T synthesis to 24 h provided evidence of such a proposal that the 24 h + 5 min sample showed a crystal size approximately 50 nm, similarly sized to the low-T synthesized sample (milled-72 h, Figure 2.2c; for convenient comparison, here after, designated as 72 h + 0 min). Therefore, the two-stage synthesis resulted in nanosized zeolite with controllable crystal size within the order of minutes. Further, the low-T synthesis played important role in prohibiting unnecessary Ostwald ripening, while the high-T treatment remarkably accelerated the crystal growth process.
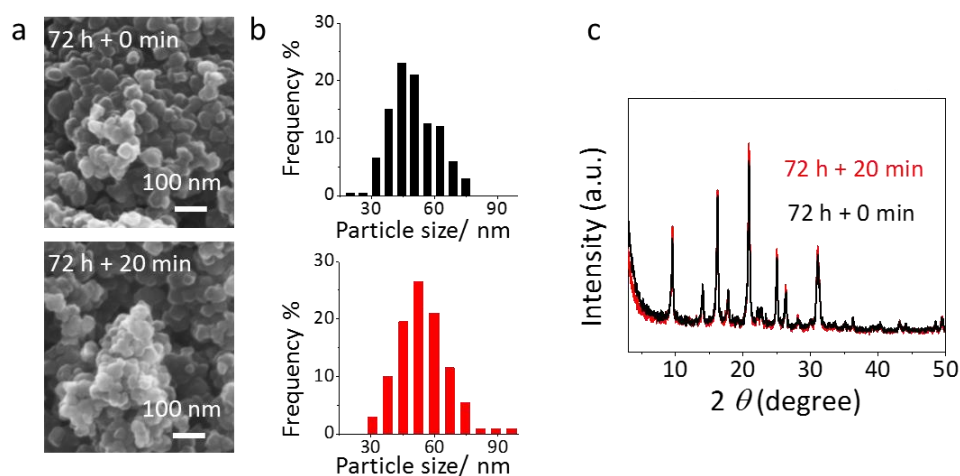
Figure 2.5 Additional high-T treatment on fully crystallized sample under low-T condition: a, SEM images of 72 h + 0 min and 72 h + 20 min. b, crystal size distributions. c, XRD patterns.

It is worth noting that, different from the previous nanosized SSZ-13 obtained under low-T synthesis, all the two-stage synthesized nanosized samples showed 100% relative crystallinity, which is comparable with the raw seed. Since 72 + 0 min sample proved to be full crystallized under low-temperature, a further high-T treatment was imposed on it to clarify the effects of high temperatures. The obtained sample is designated as 72 h + 20 min. No increase in the solid yield (12.6% *vs.* 11.7%) was observed after such kind of additional high-T treatment, as well as the crystal size distributions (Figure 2.5a and b). However, a surprising increase of the crystallinity was verified by XRD patterns (Figure 2.5c), which is in line with the calculated relative crystallinity from about 84% to 100% (Figure 2.2a). Thus, the high-T treatment in this two-stage synthesis promoted the formation of more ordered crystalline structures.

2.3.4 Hydrothermal stability of nanosized zeolites synthesized in two-stage route

A similar hydrothermal stability test was performed on the nanosized SSZ-13 zeolites obtained through the two-stage synthesis (also raw seed was used as standard). As shown in Figure 2.6a, An obvious trend is that with longer high-T treatment, the sample shows stronger resistance to the hydrothermal degradation. The 0 h + 60 min shows considerably high residual crystallinity even after hydrothermal treatment at 700 ℃ and 800 ℃ for 5 h (95% and 80%, respectively), despite of its relatively wider crystal size distribution. For the other uniform nanosized SSZ-13, their hydrothermal stability is also enhanced to different extent, depending on the synthesis periods at high-T stage (12 h + 20 min and 24 h + 5min). Moreover, as above discussed, an additional high-T stage is even effective on the fully crystallized sample in low-T synthesis (72 h + 0 min and 72 h + 20 min), their degradation behaviors further confirmed the effectiveness of high-T stage for enhancing hydrothermal stability of nanosized zeolites (Figure 2.6b). The summarized properties of all these samples are shown Table 2.1.
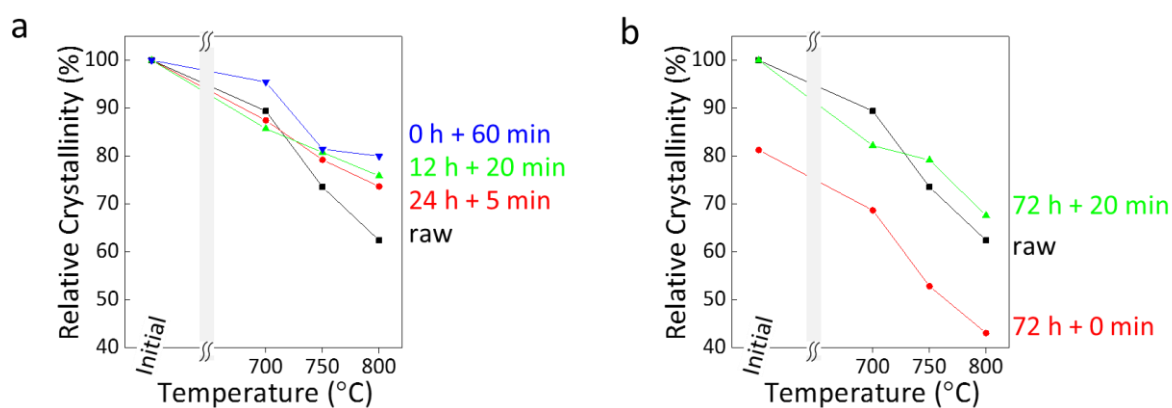
Figure 2.6 Degradation curves of raw seed and two-stage synthesized SSZ-13 zeolite: a, raw seed, 24 h + 5 min, 12 h + 20 min, 0 h + 60 min. b, raw seed, 72 h + 0 min, 72 h + 20 min.

Table 2.1 Properties and hydrothermal stabilities of the SSZ-13 zeolite

Sample	Si/Al[a]	Particle size (nm)[b]	Micropore volume (cm³g⁻¹)[c]	Degradation residues (after 800 ℃)	
				Micropore volume[d]	Crystallinity[e]
Raw	15.0	1000–2000	0.30	61 %	62 %
0 h + 60 min	16.5	60–300	0.29	88 %	80 %
12 h + 20 min	15.4	50–150	0.29	81 %	76 %
24 h + 5 min	14.6	~50	0.27	72 %	74 %
72 h + 0 min	14.5	~ 50	0.26	56 %	53 %
72 h + 20 min	15.0	~ 50	0.28	69%	68 %

a. Determined by ICP.

b. Evaluated from SEM images.

c. Determined by the *t*-plot method.

d. Compared before and after hydrothermal treatment at 800 ℃ by the *t*-plot method.

e. Compared before and after hydrothermal treatment at 800 ℃ from XRD patterns.

2.3.5 HEXTS and solid-stage ²⁹Si and ²⁷Al NMR measurements

To clarify how the high-T synthesis had affected the zeolite structures that finally resulted in the enhanced hydrothermal stability of nanosized zeolites, HEXTS measurements were performed to verify the possible changes of relative positions of atoms (Figure 2.7a). Several atomic distances were identified in the pair distribution functions $G(r)$ (derived from the total structural factors $S(Q)$, Figure 2.7b). The peaks at 1.6, 2.6, and 3.1 Å are assigned to the first nearest distance of T–O, O–O, and T–T, respectively (T = Si or Al), and no significant difference is observed, regardless of the shape and size in different samples.[27-28] The peaks distributed at 3.6–4.0 Å and 4.0–4.3 Å mainly correspond to the second-nearest neighbor of T–O in the 4-, 6- and 8-membered rings and of T–T in the 4-membered rings, respectively. No obvious peak shift occurs when the raw seed and the 12 h + 20 min samples are compared, while significant peak shifts can be observed for 72 h + 0 min sample at the 2nd T-O sites for 4-6-8 membered rings (Figure 2.7a, blue arrows). As discussed in previous paper, as crystallization, the distorted membered rings would extend to accommodate the formation of

zeolite framework. As a result, the T–O and T–T peaks would shift to longer distances.[28] Herein, despite the unchanged crystallinity under low-T for a considerably long period (72–168 h, Figure 2.2a), the 72 h + 0 min sample behaved a partially distorted structures similar to the milled SSZ-13.[23] This may explain the its inferior performance during hydrothermal stability test. However, after an additional high-T synthesis treatment, the peak corresponding to the 2nd T-O at 4 membered rings bounce back, indicating a healing effect from the high-T treatment on the originally distorted structures.

As the observed changes of relative positions of T-atoms, solid state NMR was expected to be useful for further illuminate the coordinated conditions of Si and Al species in different samples (Figure 2.8). The raw SSZ-13 zeolite has a typical ^{29}Si NMR spectrum of high silica SSZ-13 with 3 peaks attributed to $Si(OSi)_4$, $Si(OAl)(OSi)_3$ and $Si(OAl)_2(OSi)_2$ species (Figure 2.8a). However, considering the difference between calculated Si/Al ratio based on NMR (*e.g.*, for raw seed Si/Al=6.9) and ICP (*e.g.*, for raw seed Si/Al=15), there must be some silanol defects presented in the structure which were not confirmed by the CP/MAS NMR. Thus, the peaks at δ = -99 ppm are assigned to Q_4 (2Al) sites together with Q_3 defects. Contents of these different Si species are also given for comparison (Figure 2.8a). Obviously, the sample prepared at low temperature possesses more defects (72 h + 0 min, Q_4 (2Al) + Q_3 defects = 25%), while after high-T treatment, the defects can be partially healed (72 h + 20 min, Q_4 (2Al) + Q_3 defects = 19%). No significant difference can be observed between raw seed and the 12 h + 20 min.
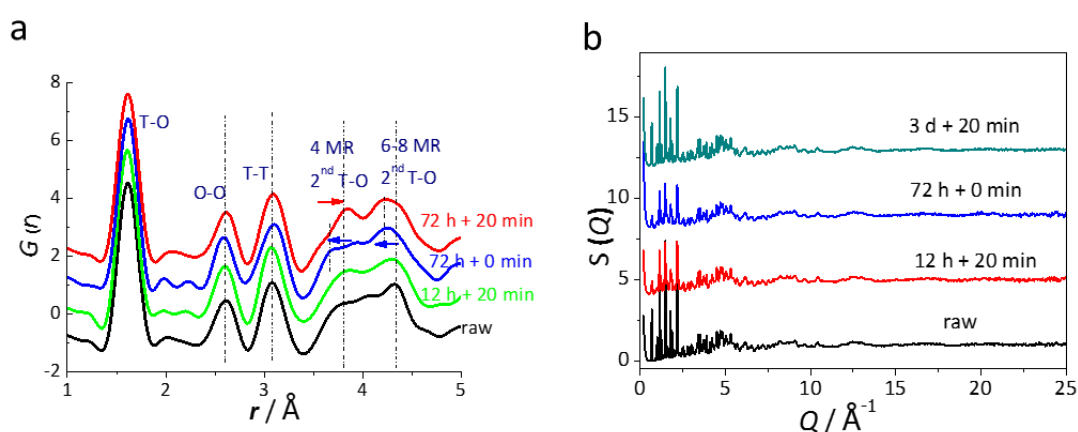
Figure 2.7 Pair distribution function, $G(r)$ (a) and total structure factors, $S(Q)$ (b) derived from HEXTS of raw, 12 h + 20 min, 72 h + 0 min, and 72 h + 20 min samples.
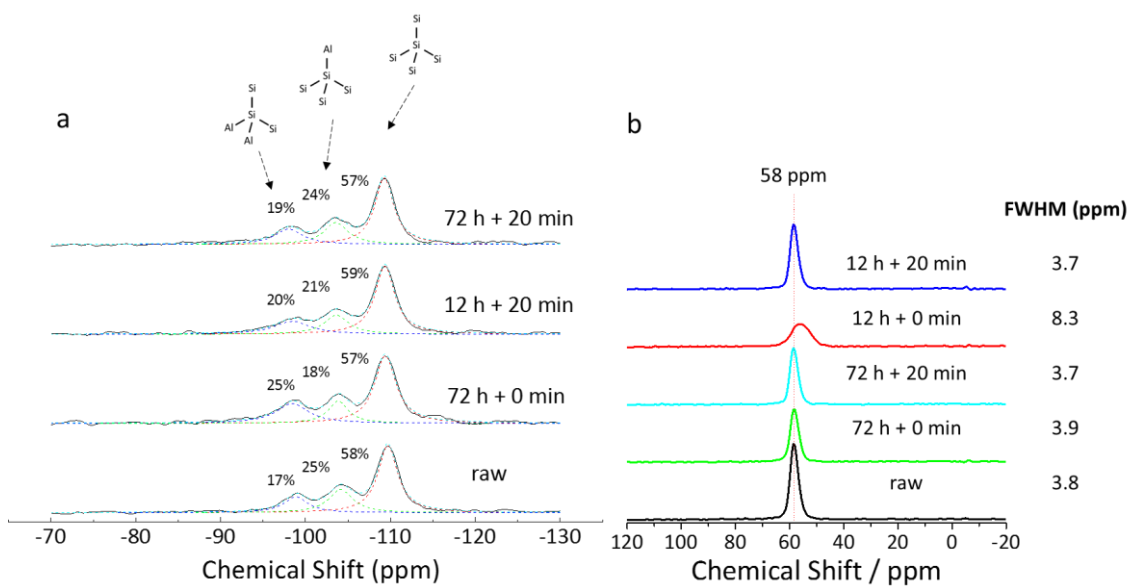
Figure 2.8 ^{29}Si (a) and ^{27}Al NMR (b) of raw seed and two-stage synthesized SSZ-13 zeolites

All the ^{27}Al NMR spectra display a single peak between 50 and 60 ppm, which is typically assigned to the presence of tetrahedrally coordinated Al species (Figure 2.8b). The full width at half maximum heights (FWHM) that strongly depends on the local ordering of the Al atoms are also shown here. As the 12 h + 0 min sample is almost amorphous, it shows a pretty wide FWHM. With additional high-T treatment, the shift and sharpening of the peak imply the rapid formation of a crystalline structure (12 h + 20 min). On the other hand, the 72 h + 0 min sample that shows relatively lower crystallinity has a slightly broader peak than those of the raw seed and the 12 h + 20 min sample. Benefited from the addition of high-T treatment for 20 min, the FWHM was only marginally reduced (from 3.9 to 3.7), being consistent with the increase in the diffraction peaks as shown in Figure 2.5c. All these solid-state NMR results indicate reasonable changes compared with the HEXTS results that under low-T synthesis condition, more defects as well as distorted crystalline structures are favored to be formed, which corresponding for the relatively inferior structural stability of the obtained nanosized zeolite; after the following high-T synthesis treatment, the above mentioned structural disadvantages are healed to some extent, depending on the detailed treatments. If an appropriate two-stage synthesis was applied, nanosized zeolites with excellent hydrothermal stability would be obtained in short periods, indicating a very efficient way to prepare the zeolite materials with desired properties.

2.3.6 Catalytic performance of nanosized zeolites with excellent hydrothermal stability

Combustion of fossil fuels has inevitably led to the production of air pollution, in which, nitrogen oxide (NOx) is one of the most important pollutants. Selective catalytic reduction (SCR) of NOx by NH_3 from stationary sources have shown excellent efficiency and stability as a controlling technology for that problem (Scheme 2.1). The ion-exchanged small pore zeolites such as CHA as catalysts have showed high potential to be used in this reaction.
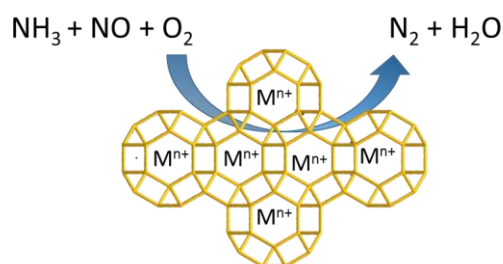
Scheme 2.1 illustration of ion-exchanged zeolite catalysts used in NH_3-SCR reaction.

To investigate the catalytic performance of the nanosized zeolite with excellent hydrothermal stability, 3 samples of raw seed, 72 h + 0 min, 12 h + 20 min were ion-exchanged for a comparable Cu^{2+} content (ca. 2.8%). As shown in Figure 2.9a, the 3 samples showed similar NO conversion trends at different reaction temperatures under fresh condition, even the 72 h + 0 min sample which showed low crystallinity and weak hydrothermal stability. However, after the hydrothermal aging for 5 h at 800 ℃, the catalytic activity of the 72 h + 0 min sample decreased sharply (Figure 2.9b), which is consistent with its remarkably decreased crystallinity and micropore volumes showed in previous discussion. On the contrary, for the nanosized SSZ-13 obtained through the two-stage synthesis (12 h + 20 min), there was no loss in catalytic performance compared to that of raw SSZ-13, which further verified the enhanced hydrothermal stability.
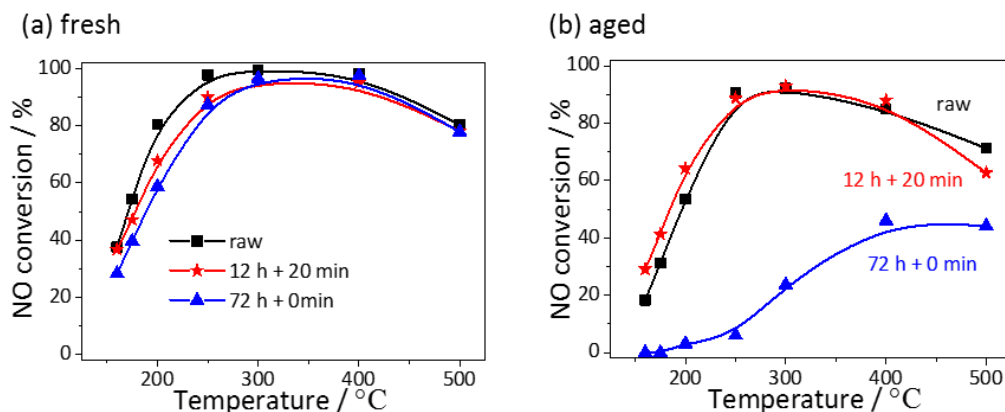
Figure 2.9 NO conversion over Cu-loaded (ca. 2.8wt%) CHA zeolite catalysts: (a) fresh conditions, (b) after hydrothermal aging for 5 h at 800 ℃.

2.3.7 Crystallization pathway of nanosized SSZ-13 zeolite under two-stage synthesis condition

In this Chapter, a two-stage synthesis including a low-T synthesis and a following high-T synthesis is presented by which, nanosized SSZ-13 zeolite with enhanced hydrothermal stability can be obtained in short periods. In low-T synthesis stage, the interaction between added seed and other organic or inorganic species were enhanced that a uniform precursor having large amounts of nucleation was prepared; while in high-T synthesis stage, the crystal growth was accelerated remarkably. Thanks to both of the uniform precursor formed before high-T treatment and the ultrashort periods needed under high temperatures, the generally occurred Ostwald ripening was suppressed that nanosized SSZ-13 zeolite with narrow crystal size distribution can be facilely controlled by the two temperature programs. A summarized pathway for the two-stage synthesis is shown in Scheme 2.2, in which 3 different routes are displayed based on the different periods maintained at either stage. As the presence of the milled seed, the nucleation occurs as a secondary nucleation which is induced by the easily dissolved seed species. In high temperature treatment alone (Scheme 2.2, route 1), fast crystal growth would simultaneously start from partially dissolved seeds as well as the secondary nuclei. The morphology evolutions from 0 h + 5 min to 0 h + 60 min are shown in Figure 2.10. After 30 min of high-T treatment, an obvious differentiation of particle size was observed. Consequently, due to further crystal growth and the Ostwald ripening under high synthesis temperature, the size distribution of the products (0 h + 60 min) would be widened. On the other hand, when the synthesis proceeds at low temperature for a sufficiently long period (*e.g.,* 95 ℃,

route 2), the seed dissolves constantly and performs interaction with the mother liquor, allowing formation of uniform, secondary nuclei before crystal growth starts. However, the low-T treatment results in many structural defects in the nanosized SSZ-13 zeolites, which degrade their hydrothermal stabilities as discussed above. Finally, a two-stage synthesis under controlled temperature and duration was proposed (route 3). The first low-T stage promises a narrow size distribution of crystal at the initial moment of crystal growth, and the second high-T stage realizes fast synthesis within a few minutes (*e.g.*, 24 h + 5 min, 12 h + 20 min) as well as helps heal the structural defects generated during the low-T stage.

Route	Size distribution	Hydrothermal stability
1	Uneven	Good
2	Uniform	Poor
3	Uniform	Good
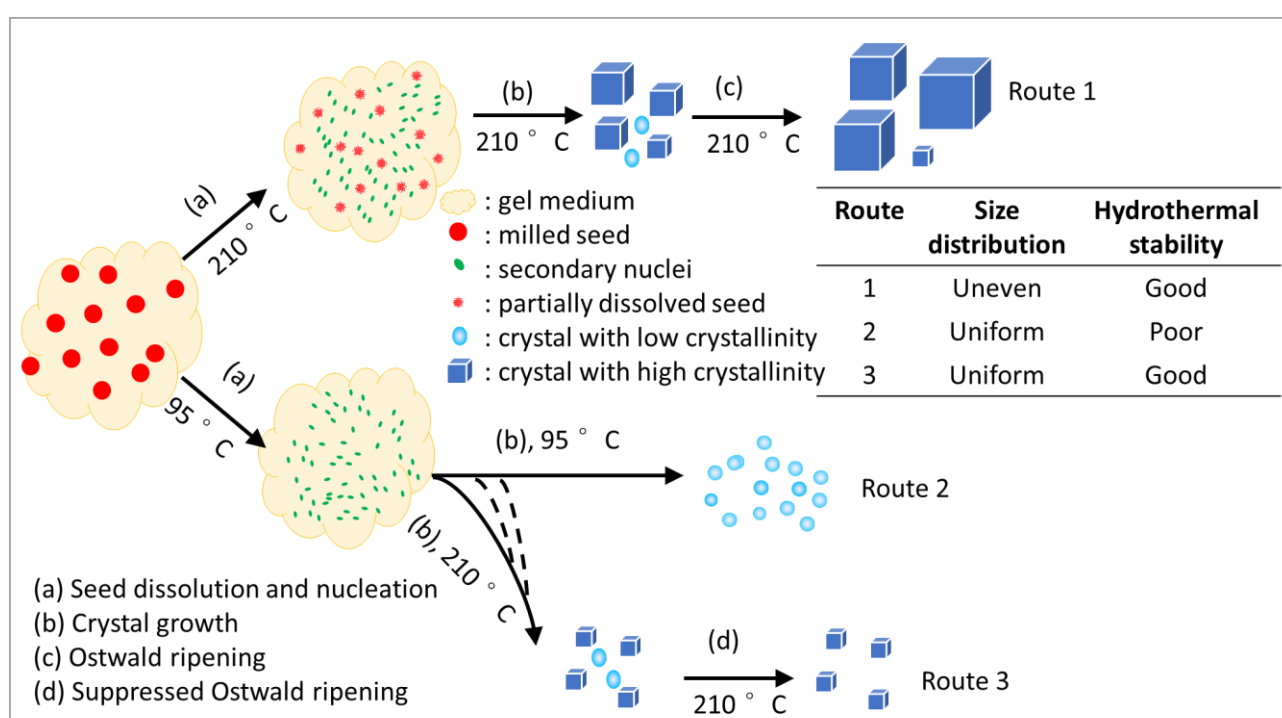
Scheme 2.2 Schematic pathways of two-stage synthesis for nanosized SSZ-13 zeolite with enhanced hydrothermal stability.
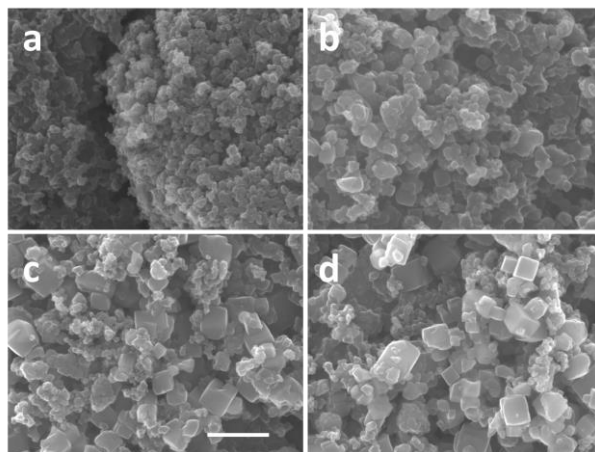
Figure 2.10 SEM images of 0 + 5 min, 0 + 10 min, 0 + 30 min, 0 + 60 min (a–d, respectively). The scale bar is 500 nm.

2.4 Summary

This chapter demonstrated an efficient direct-synthesis method to tune the hydrothermal stability and crystal size of zeolite catalysts. The namely two-stage synthesis should be firstly conducted under a relatively low temperature (*e.g.* 95 ℃) for several hours, through which, homogeneous precursor can be obtained. Then after, an ultrashort treatment under high temperature (*e.g.* 210 ℃ for several minutes) will be imposed for an ultrafast crystal growth. Several adjustments were introduced into this approach to realize such kind of improvements: i) addition of milled seed followed by low-T treatment not only contributes to the skip of rather long induction period but also allows large amounts of nucleation in a uniform way. ii) the employment of high-synthesis temperature accelerates the crystal growth considerably and further, gives structural healing effects on the nucleation formed during low-T process. This established approach is a highly economic way to reach high quality zeolite materials thanks to its operability and the ultrashort periods needed.

References

[1]   S. Mintova, J.-P. Gilson, V. Valtchev, Advances in nanosized zeolites, *Nanoscale* **2013**, 5, 6693-6703.

[2]   H. Awala, J.-P. Gilson, R. Retoux, P. Boullay, J.-M. Goupil, V. Valtchev, S. Mintova, Template-free nanosized faujasite-type zeolites, *Nat. Mater.* **2015**, 14, 447.

[3]   R. Mart ńez-Franco, C. Paris, M.E. Mart ńez-Armero, C. Mart ńez, M. Moliner, A. Corma, High-silica nanocrystalline Beta zeolites: efficient synthesis and catalytic application, *Chem. Sci.* **2016**, 7, 102-108.

[4]   X. Zhang, D. Liu, D. Xu, S. Asahina, K.A. Cychosz, K.V. Agrawal, Y. Al Wahedi, A. Bhan, S. Al Hashimi, O. Terasaki, Synthesis of self-pillared zeolite nanosheets by repetitive branching, *Science* **2012**, 336, 1684-1687.

[5]   Y. Kim, K. Kim, R. Ryoo, Cooperative structure direction of diammonium surfactants and sodium ions to generate MFI zeolite nanocrystals of controlled thickness, *Chem. Mater.* **2017**, 29, 1752-1757.

[6]   H.Y. Luo, V.K. Michaelis, S. Hodges, R.G. Griffin, Y. Rom án-Leshkov, One-pot synthesis of MWW zeolite nanosheets using a rationally designed organic structure-directing agent, *Chem. Sci.* **2015**, 6, 6320-6324.

[7]   M. Kumar, H. Luo, Y. Román-Leshkov, J.D. Rimer, SSZ-13 crystallization by particle attachment and deterministic pathways to crystal size control, *J. Am. Chem. Soc.* **2015**, 137, 13007-13017.

[8]   Z. Chen, S. Li, Y. Yan, Synthesis of template-free zeolite nanocrystals by reverse microemulsion− microwave method, *Chem. Mater.* **2005**, 17, 2262-2266.

[9]   T. Wakihara, A. Ihara, S. Inagaki, J. Tatami, K. Sato, K. Komeya, T. Meguro, Y. Kubota, A. Nakahira, Top-down tuning of nanosized ZSM-5 zeolite catalyst by bead milling and recrystallization, *Cryst. Growth Des.* **2011**, 11, 5153-5158.

[10]   Z. Liu, N. Nomura, D. Nishioka, Y. Hotta, T. Matsuo, K. Oshima, Y. Yanaba, T. Yoshikawa, K. Ohara, S. Kohara, T. Okubo, T. Wakihara, A top-down methodology for ultrafast tuning of nanosized zeolites, *Chem. Commun.* **2015**, 51, 12567-12570.

[11]   C. Anand, Y. Yamaguchi, Z. Liu, S. Ibe, S.P. Elangovan, T. Ishii, T. Ishikawa, A. Endo, T.

Okubo, T. Wakihara, Pioneering In Situ Recrystallization during Bead Milling: A Top-down Approach to Prepare Zeolite A Nanocrystals, *Sci. Rep.* **2016**, 6, 29210.

[12]   H. Yamada, T. Iida, Z. Liu, Y. Naraki, K. Ohara, S. Kohara, T. Okubo, T. Wakihara, Downsizing AFX Zeolite Crystals to Nanoscale by a Postmilling Recrystallization Method, *Cryst. Growth Des.* **2016**, 16, 3389-3394.

[13]   S. Zheng, A. Jentys, J.A. Lercher, On the enhanced para-selectivity of HZSM-5 modified by antimony oxide, *J. Catal.* **2003**, 219, 310-319.

[14]   T. Zhang, J. Shi, J. Liu, D. Wang, Z. Zhao, K. Cheng, J. Li, Enhanced hydrothermal stability of Cu-ZSM-5 catalyst via surface modification in the selective catalytic reduction of NO with NH3, *Appl. Surf. Sci.* **2016**, 375, 186-195.

[15]   H. Gies, B. Marker, The structure-controlling role of organic templates for the synthesis of porosils in the systems SiO_2/template/H_2O, *Zeolites* **1992**, 12, 42-49.

[16]   B. Bayati, A. Babaluo, R. Karimi, Hydrothermal synthesis of nanostructure NaA zeolite: The effect of synthesis parameters on zeolite seed size and crystallinity, *J. Eur. Ceram. Soc.* **2008**, 28, 2653-2657.

[17]   Y. Zou, R. Wang, Z. Zhang, G. Li, S. Qiu, Synthesis of thermal stable mesoporous titanosilicates assembled from titanosilicates precursors at high temperature, *Micropor. Mesopor. Mater.* **2013**, 182, 178-184.

[18]   T. Takata, N. Tsunoji, Y. Takamitsu, M. Sadakane, T. Sano, Nanosized CHA zeolites with high thermal and hydrothermal stability derived from the hydrothermal conversion of FAU zeolite, *Micropor. Mesopor. Mater.* **2016**, 225, 524-533.

[19]   J.H. Kwak, R.G. Tonkyn, D.H. Kim, J. Szanyi, C.H. Peden, Excellent activity and selectivity of Cu-SSZ-13 in the selective catalytic reduction of NOx with NH3, *J. Catal.* **2010**, 275, 187-190.

[20]   F. Bleken, M. Bjørgen, L. Palumbo, S. Bordiga, S. Svelle, K.-P. Lillerud, U. Olsbye, The effect of acid strength on the conversion of methanol to olefins over acidic microporous catalysts with the CHA topology, *Top. Catal.* **2009**, 52, 218-228.

[21]   A. Hwang, M. Kumar, J.D. Rimer, A. Bhan, Implications of methanol disproportionation on catalyst lifetime for methanol-to-olefins conversion by HSSZ-13, *J. Catal.* **2017**, 346, 154-160.

[22]   S.I. Zones, L.-T. Yuen, S.J. Miller, Small crystallite zeolite CHA, Google Patents2004.

[23]   Z. Liu, T. Wakihara, K. Oshima, D. Nishioka, Y. Hotta, S.P. Elangovan, Y. Yanaba, T. Yoshikawa, W. Chaikittisilp, T. Matsuo, T. Okubo, T. Wakihara, Widening Synthesis Bottlenecks: Realization of Ultrafast and Continuous-Flow Synthesis of High-Silica Zeolite SSZ-13 for NOx Removal, *Angew. Chem. Int. Ed.* **2015**, 54, 5683-5687.

[24]   F. Gao, E.D. Walter, E.M. Karp, J. Luo, R.G. Tonkyn, J.H. Kwak, J. Szanyi, C.H. Peden, Structure-activity relationships in NH3-SCR over Cu-SSZ-13 as probed by reaction kinetics and EPR studies, *J. Catal.* **2013**, 300, 20-29.

[25]   K. Iyoki, K. Itabashi, T. Okubo, Progress in seed-assisted synthesis of zeolites without using organic structure-directing agents, *Micropor. Mesopor. Mater.* **2014**, 189, 22-30.

[26]   S. Zones, Conversion of faujasites to high-silica chabazite SSZ-13 in the presence of N, N, N-trimethyl-1-adamantammonium iodide, *J. Chem. Soc. Faraday Trans.* **1991**, 87, 3709-3716.

[27]   T. Wakihara, S. Kohara, G. Sankar, S. Saito, M. Sanchez-Sanchez, A.R. Overweg, W. Fan, M. Ogura, T. Okubo, A new approach to the determination of atomic-architecture of amorphous zeolite precursors by high-energy X-ray diffraction technique, *Phys. Chem. Chem. Phys.* **2006**, 8, 224-227.

[28]   W. Fan, M. Ogura, G. Sankar, T. Okubo, In situ small-angle and wide-angle X-ray scattering investigation on nucleation and crystal growth of nanosized zeolite A, *Chem. Mater.* **2007**, 19, 1906-1917.

[29]   C. Peng, Z. Liu, A. Horimoto, C. Anand, H. Yamada, K. Ohara, S. Sukenaga, M. Ando, H. Shibata, T. Takewaki, Preparation of nanosized SSZ-13 zeolite with enhanced hydrothermal stability by a two-stage synthetic method, *Micropor. Mesopor. Mater.* **2018**, 255, 192-199.

Chapter 3 Ultrafast Post-Synthesis of Core-shell Structured ZSM-5@Silicalite-1 Zeolite

3.1 Introduction

The acidity of zeolites is attributed to the Brønsted acid sites, which is located on the oxygen atoms bridging Si and Al atoms. In practical reactions, the acid sites located in confined micropores impose shape selectivity for both reactants and products.[1] However, the desired selective conditions can be altered by the presence of non-selective external acid sites.[2] Especially when nanosized zeolites are used due to their advantages in shorter diffusion pathway, the simultaneously increased surface acidity could inflict some undesired effects.

To address aforementioned problems, a surface passivation technology was firstly proposed by Mobil in 1970s, when they tried to deposit a silica layer on the external surface of ZSM-5 zeolite.[3] Starting from which, post-synthesis treatments aiming at tailoring the surface acidity of zeolites have been developed extensively due to the low cost as well good operability. Typical examples include the chemical vapor or liquid deposition (CVD or CLD), through which, various functional groups such as metal oxides, hydride, alkyl, or alkoxy compounds were chemisorbed on the zeolite surface.[4-7] These methods help enhance the shape selectivity by eliminating the surface acidity and narrowing the pore mouth openings. However, the concurrently occurred pore blockage and increased internal diffusion resistance present as the main drawbacks.

Preparation of core-shell structures have been commonly accepted as an effective strategy for functional materials with applications in wide fields such as drug delivery systems, semi-conductors, and catalysis.[8-10] Growing a designed zeolitic shell on an existing zeolite core by post-synthesis treatment, which yields a core-shell structured zeolite composite, has been thought to be an effective way to circumvent the aforementioned problems during surface passivation.[11] Due to the rich diversity of porous structures and compositions, the proper combinations of the zeolite core and shell are expected to possess tunable acidity, well-preserved hydrothermal stability, and dual functionality. There have been tremendous reports regarding the preparation of core-shell structured zeolites such as EMT@FAU, SOD@CAN, SOD@CHA, MOR@MFI, SOD@LTA, BEA@LTA, FAU@MFI,

FAU@BEA, BEA@MFI, MFI@BEA, and MFI@MFI. [11–18] The preparation methods can be divided into two approaches: epitaxial overgrowth and seed-induced secondary growth. In epitaxial overgrowth, the connectivity between the shell and core is limited by specific compatibility via heteroepitaxial or homoepitaxial characteristics.[12, 13] In seed-induced secondary growth, nanosized seeds from the shell zeolite were preliminarily adsorbed onto the core zeolite surface followed by secondary crystal growth.[11, 14] However, for either approach, the coating process takes a considerably longer time under hydrothermal conditions similar to the scenarios for zeolite synthesis, *e.g.*, from several hours to even a few days. Thus, a high demand exists for the development of an ultrafast method to prepare these core-shell structured zeolites.

In previous chapter, ultrafast direct-synthesis by controlling the two-stage temperature programs was proposed to be an effective way to obtain nanosized SSZ-13 zeolite with excellent hydrothermal stability.[19] In this chapter, to develop an ultrafast post-synthesis treatment for passivating the surface acidity of zeolites, some similar factors including the high temperature, reactor featuring fast heating are also included in current context. ZSM-5 having MFI-type structure is one of the most frequently used zeolite catalysts. This catalyst has widespread applications in shape-selective catalysis such as toluene disproportionation and toluene methylation to yield *para*-xylene.[20] Forming a crystalline, porous silicalite-1 shell onto the ZSM-5 zeolite has shown considerable effectiveness for enhancing its catalytic selectivity.[21] Here, an ultrafast post-synthesis of coating a silicalite-1 shell on ZSM-5 core is presented.[22] Moreover, this ultrafast process showed considerable flexibility that precise control on the shell thickness can be realized easily. Finally, based on analyzing the requirements for an ultrafast post-synthesis for core-shell structured zeolite, a continuous flow reaction system was successfully established. The main contents of this chapter has been published in reference 28.

3.2 Experiment

3.2.1 Materials and tools

The following chemicals were used as received without any further purification: tetraethoxysilane (TEOS), sodium hydroxide (NaOH), aluminum hydroxide (Al(OH)$_3$; Wako Pure Chemical Industries, Ltd.), colloidal silica (LUDOX®AS-40, Sigma-Aldrich), and tetrapropylammonium hydroxide (TPAOH, 40 wt. %, Merck).

3.2.2 Synthesis of ZSM-5 core

The ZSM-5 core was synthesized with a modified reaction composition of 1 SiO_2: 0.033 Al_2O_3: 0.167 NaOH: 0.067 TPAOH: 7.67 H_2O using a Teflon®-lined stainless steel autoclave (#4749, Parr Instrument Company). For a typical process, the TPAOH solution and NaOH (aq. 20 wt. %) were firstly mixed, followed by the addition of the aluminum source. After 10 min of dispersion under stirring, the silica source was added drop wise to the solution. After a further stirring for 30 min, 10 g of the mixed reactants were transferred into the autoclave and aged at 60 ℃ under static condition for 24 h. The autoclave was then hydrothermally treated at 150 ℃ for another 24 h for full crystallization. The product was recovered by centrifugation at 14,000 rpm for 10 min, thoroughly washed with water, and dried at 80 ℃ overnight. The as-synthesized ZSM-5 was used directly without prerequisite calcination or ion-exchange.

3.2.3 Ultrafast preparation of core-shell structured ZSM-5@Silicalite-1

The synthesis solution for silicalite-1 shell was prepared by mixing TEOS, TPAOH, and water with a composition of 1 SiO_2: 0.3 TPAOH: 120 H_2O: 4 EtOH. After 2 h of stirring for hydrolysis of TEOS in the alkaline environment, the ZSM-5 core (amount determined as SiO_2 (core): SiO_2 (shell) = 1:1) was added followed by stirring for another hour. Reactants were then transferred into the tuber reactor (*o.d./i.d.* = 10.0/8.0 mm)and heated at 190 ℃ for 0–10 min in a pre-heated oil bath.

3.2.4 Continuous flow synthesis of core-shell structured ZSM-5@Silicalite-1

Teflon® (*o.d./i.d.* = 4.0/2.0 mm) and stainless (*o.d./i.d.* = 6.6/4.4 mm) tubes were combined as the continuous flow reactors, in which, the reactant mixtures went through the Teflon® tube with the assistance of a high pressure syringe pump, while the hot water (210 ℃) was fed into the stainless tube as a heating source. The cooling water was supplied by a HPLC pump (MP311, Lab-Quatec, Japan) to dilute and cool the fluid after reaction. The system pressure were controlled by a back pressure regulator (TESCOM 26-1700, Emerson, US). The pressure and temperature changes at each part of the system were recorded by a homemade digital system for visualization. Safety valves were attached with the systems.

3.2.5 Cracking of (1-methylethyl)-benzene (cumene) and 1,3,5-triisopropylbenzene (TIPB)

In order to evaluate the activity for Brønsted acid-catalyzed reaction, cracking of (1-methylethyl)-benzene (cumene) was carried out according to a previous study in a pulse method. [27] The sample (10 mg) was packed in a Pyrex tube (4 mm inner diameter), pre-treated in a He flow (ca. 200 kPa, 37 μmol s-1) at 773 K for 1 h, and then a pulse of cumene (7.2 μmol) was fed at 523 K. The outlet of reactor was directly connected to a column of Silicone SE30, and the products were analyzed with an FID-GC. Most of the products were propene and benzene. The catalytic activity is shown by the conversion of cumene in the first pulse. The conversion was calculated using following equation:

$$\text{Conversion (\%)} = \left(1 - \frac{\text{carbon in cumene}}{\text{carbon in propene, benzene, cumene}}\right) \times 100\% \quad \text{(Equation 1)}$$

In order to evaluate the extent of Brønsted acid site inactivation on external surfaces, the catalytic activity for 1,3,5-TIPB, cracking was measured based on analytical details from a previous study.[28] The catalyst sample (5 mg) was packed in a Pyrex tube (4 mm inner diameter), pre-treated in an He flow (ca. 200 kPa, 20 μmol s^{-1}) at 773 K for 1 h, and then a pulse of 1,3,5-TIPB (4.1 μmol) was fed to the tube at 673 K. The reactor outlet was directly connected to a silicone SE30 column, and the products were analyzed with a FID-GC. Most products were propene and benzene, with a small amount of cumene (isopropylbenzene) and 1,3-diisopropylbenzene. Catalytic activity is characterized by 1,3,5-TIPB conversion in the first pulse. The conversion was calculated using the following equation：

$$\text{Conversion (\%)} =$$
$$\left(1 - \frac{\text{carbon in TIPB}}{\text{carbon in propene, cumene, 1,3} - \text{disisopropylbenzene, TIPB}}\right) \times 100\% \quad \text{(Equation 2)}$$

This equation assumes that the amount of C (carbon atom) is proportional to peak intensity in the chromatogram recorded by the FID-GC.

3.2.6 Characterization

Transmission electron microscopy (TEM) images were taken on a JEM-2000EX (JEOL, Japan) under a working voltage of 102 kV. Nitrogen adsorption–desorption measurements were performed on a Quantachrome Autosorb-iQ2 instrument at liquid nitrogen temperature with an outgas pretreatment at 325 ℃ for 4 h under vacuum. Solid-state MAS NMR spectra were collected with a

JEOL ECA 500 spectrometer. The ^{27}Al MAS NMR spectra were recorded at 130.33 MHz with a 3.2 μs π/2 pulse length, a 5 s recycle delay, and a spinning frequency of 14 kHz. The ^{29}Si MAS NMR spectra were recorded at 99.37 MHz with a 5.0 μs π/2 pulse length, a 60 s recycle delay, and a spinning frequency of 10 kHz. The XPS measurements were performed on a JEOL JPS-9000 instrument using MgKα radiation and calibrated using a C1s binding energy of 284.8 eV (assigned to adventitious carbon). XRD, SEM, TG-DTG, and ICP measurements were performed on the same equipment as described in chapter 2.

3.3 Results and discussions

3.3.1 Ultrafast post-synthesis for core-shell structured ZSM-5@Silicalite-1

The addition of silicalite-1 shell onto the ZSM-5 core was performed under 190 ℃ for 0–10 min. A summarized comparison between the core and coated samples (for 10 minutes) are shown Figure 3.1 and Table 3.1. The XRD patterns verify all the peaks belong to MFI structure (Figure 3.1a), indicating that no other kind of crystalline structures was formed during such a short periods. Isotherm of the core shows sharp increase at range of $P/P_0 = 0.9$–1.0 (Figure 3.1b), indicating the presence of interstices among small crystals. This result is consistent with the rough surface morphology of the core (Figure 3.1c), which is typical for ZSM-5 zeolite with high Al contents. After coating treatment, no significant decrease of microporosity is observed (Table 3.1), which promises the unblocked surface pore openings. However, it is worth noting that significant changes regarding the crystal size (260 vs. 390 nm) as well as the bulk Si/Al ratio (26 vs. 50). Considering the equal molar composition of SiO_2 in ZSM-5 core and silicalite-1 shell solution, this bulk Si/Al ratio incensement is quite reasonable. Moreover, the surface Si/Al ratio of coated sample shows an even higher value of 218 indicating the formation of a high-silica shell. The minor Al content is suggested to be derived from the slight dissolution of the ZSM-5 core at the very initial treatment stage. The ^{27}Al and ^{29}Si NMR results demonstrate that no further defects or octahedral extra-framework Al species were formed during the coating process (Figure 3.2a and b). When the silicalite-1 synthesis solution was directly used for hydrothermal synthesis without the addition of ZSM-5 core, the typically coffin-shaped Silicalite-1 crystal will be obtained with an average crystal size of $4 \times 2 \times 0.6$ μm (Figure 3.2c). Similar shaped morphology while with much smaller crystal size is observed on the coated samples (Figure

3.1e and f), which results in distinctively different surface morphology compared with the ZSM-5 core. Based on these results, it is suggested that silicalite-1 shell can be successfully coated onto the ZSM-5 core in very short period (*e.g.* 10 min) via this ultrafast post-synthesis treatment.

Table 3.1. A comparison of the properties before and after the coating process.

Sample	Si/Al (ICP)	Si/Al (XPS)	Size (nm) (SEM)	$V_{micro}(cm^3g^{-1})$ (*t*-plot)
Core	26	25	260	0.14
Coated	50	218	390	0.14
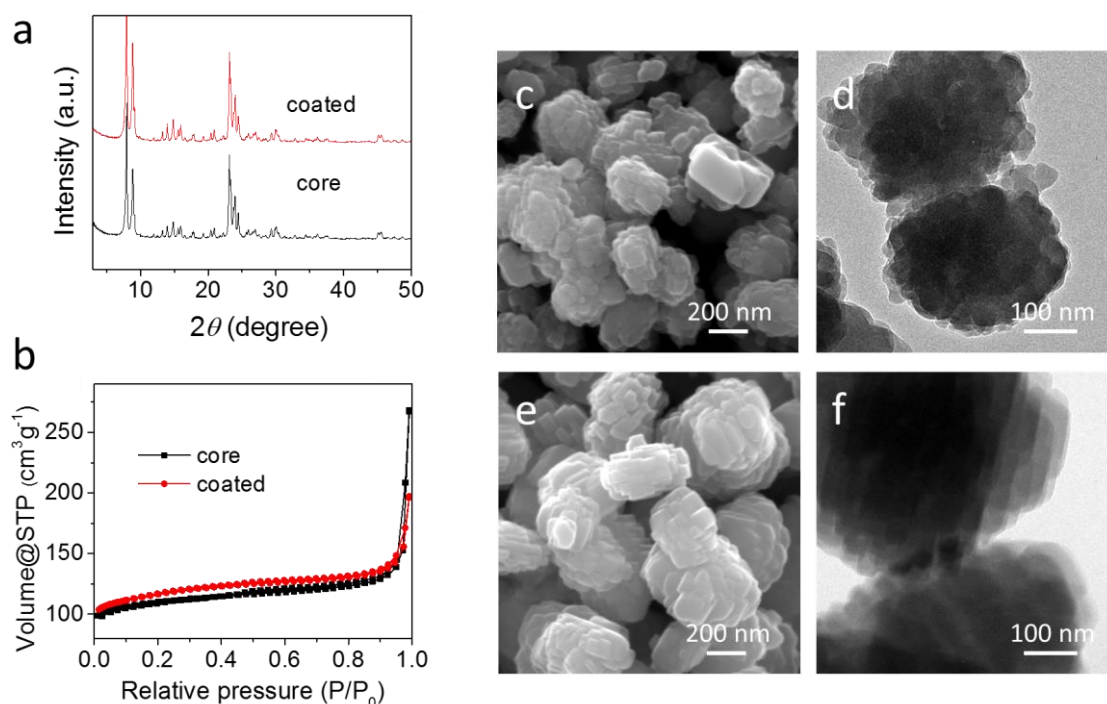
Figure 3.1 Summarized results on ZSM-5 core and coated sample for 10 min under 190 ℃. a, XRD patterns. b, N$_2$ adsorption isotherms. c and d, SEM images of core and coated samples, respectively. e and f, TEM images of core and coated samples, respectively.
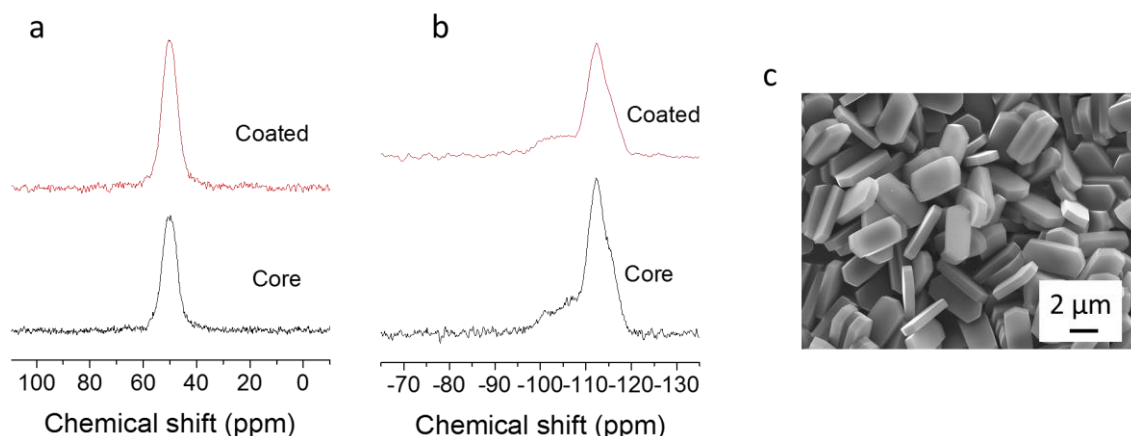
Figure 3.2 ^{27}Al NMR (a) and ^{29}Si NMR (b) spectrum for the core and coated samples. c, SEM image of Silicalite-1 crystal obtained without addition of ZSM-5 core.

3.3.2 Controllable thickness of silicalite-1 shell with treatment time effects

Due to the property dissimilarity between core and shell in core-shell structured materials, tunable shell thickness could give considerable significance in practical applications. [23, 24] With different treatment periods, controllable thickness of silicalite-1 shell can be obtained in accordance with the ultrafast crystallization process (Figure 3.3a). The concurrently increased crystal size, Si/Al ratio, and solid product yield before the culmination at 5 min indicate a continuous growth of silicalite-1 shell (Figure 3.3b). A sample estimation on the growth rate is determined as ca. 24 nm/min. This is much faster than previously reported cases of 9 nm/h [23] and 3.8 nm/h [18], in which, lower temperatures were employed. Despite the ultrafast process occurred in short periods, the gradual formation of silicalite-1 shell showed high potential in controlling the properties of the core-shell structured zeolites precisely. The gradual formation of silicalite-1 shell was further confirmed by detecting the incorporated OSDA, *i.e.* TPAOH, within the core-shell structured zeolites. All samples have nearly identical OSDA contents independent of the heating period (Figure 3.4a), which may have attributed to the sole presence of the MFI phase that for each MFI unit cell, 4 TPA$^+$ molecules are located at the channel intersections. It is worth noting that in the derivative thermo-gravimetric (DTG) curves, after 3 min of coating treatment, an additional peak at 350 ℃–425 ℃ appears and get strengthened as longer period (Figure 3.4b). Based on the analyses on the core ZSM-5 and shell silicalite-1 (Figure 3.4c), it was suggested that the 425 ℃–500 ℃ peak derives from TPA$^+$ within the ZSM-5 core, while the 350 ℃–425 ℃ peak originates from TPA$^+$ species that were incorporated into

the silicalite-1 shell due to less robust interactions between the OSDA and pure silica structure. Therefore, the gradually strengthened DTG peak located at lower temperature range was attributed to a formation of silicate-1 shell during the coating treatment.
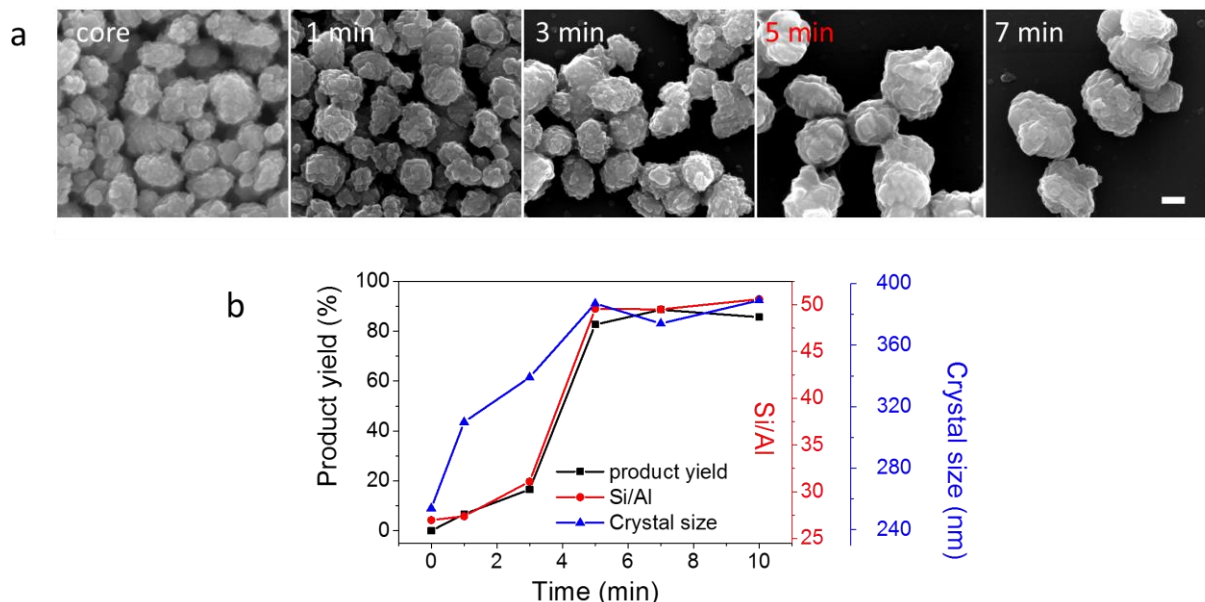
Figure 3.3 Ultrafast preparation of core-shell structured ZSM-5@Silicalite-1 for different periods (1– 10 min). a, SEM images of ZSM-5 and coated samples for different periods (1–7 min) (scale bar = 200 nm). b, SEM images of ZSM-5 and coated samples for different periods (1–7 min) (scale bar = 200 nm).
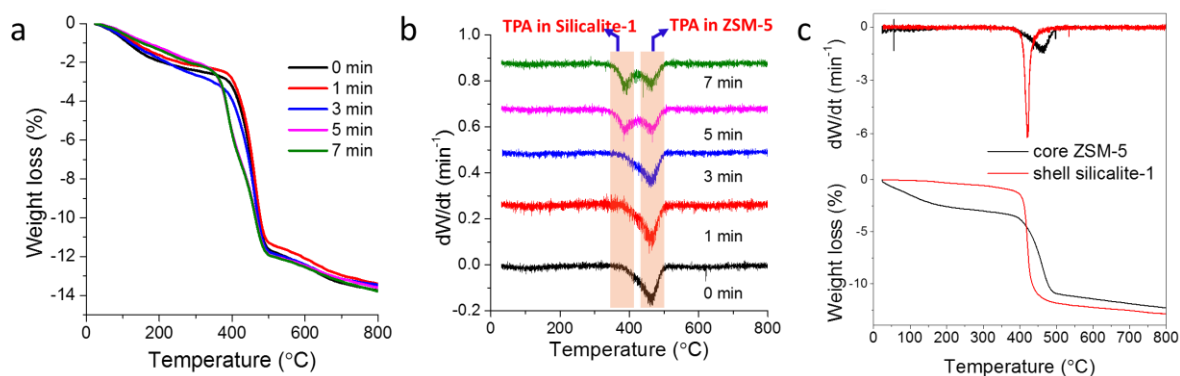
Figure 3.4 a, TGA curves of core-shell structured zeolites obtained at different periods (0– 7min). b, TG-DTG results on ZSM-5 core and shell Silicalite-1, separately. c, DTG curves of core-shell structured zeolites obtained at different periods (0– 7min).

3.3.3 Other parameters affecting the shell formation

According to the crystallization process of silicalite-1 on the surface of ZSM-5 core, the shell thickness can be facilely controlled. Besides, other kinds of way by fully consuming the Si source in silicalite-1 synthesis gel were also taken into consideration. By changing the treatment temperatures which could kinetically affect the crystallization rate and/or adjusting the amount of ZSM-5 core, this ultrafast post-synthesis for core-shell structured zeolites possesses even higher flexibility for a controllable process (Table 3.2). For instance, at higher temperatures like 210 °C, the saturated coating would be achieved in shorter periods as 3 minutes. On the other hand, increasing amounts of the ZSM-5 core not only provided more surface for secondary crystal growth but also yielded thinner silicalite-1 shells. In summary, the ultrafast coating treatment was proposed to be an efficient way for producing core-shell structured zeolites with controlled composition in short periods.

Table 3.2 Coating process under various controlled conditions.[a]

T (°C)	x	y (min)	Si/Al	Size (nm)
170	1	3	27	280
190	1	3	33	322
210	1	3	49	380
190	1	10	49	366
190	1.67	10	39	328
190	3.33	10	33	309

[a]The coating conditions are as follows: x SiO$_2$ (core): 1 SiO$_2$ (shell): 0.3 TPAOH: 120 H$_2$O, T °C for y minutes

3.3.4 Passivated external surface of core-shell structured zeolites

Cracking of TIPB and cumene were used as two probe reactions to confirm the effective removal of acidity from external surface of the core ZSM-5 and the unhindered access to Brønsted acid sites within the ZSM-5@Silicalite-1, respectively. Due to its large kinetic diameter (8.5 Å), TIPB only reacts on the external surfaces of the MFI zeolite. [24] Table 3.3 shows a dramatic reduction in TIPB cracking conversion from 79.0% to 18.4% in the first pulse reaction, which indicates reduced surface

activity after the ultrafast coating treatment (5 min). Further, when a short period of coating treatment (3 min) was applied, the coated zeolite catalyst showed correspondingly reasonable catalytic efficiency (48.3 %) with partially passivated surface. On the other hand, the cumene and its cracking products are small enough to diffuse through the micropores of MFI zeolite. The conversion of cumene was identical for all the core and coated samples (73.7%, 75.1 and 75.7%, respectively), which demonstrates that with the addition of silicalite-1 shell, the internal acid sites are still accessible. This result is consistent with the unchanged micropores volumes after coating treatment (Table 2).The above findings prove that the ultrafast preparation method for core-shell structured zeolite is successful in passivating the external surface while maintaining the original micropore accessibility.

Table 3.3 The textural properties and catalytic performance of the ZSM-5 core and the coated samples in catalyzing different cracking reactions

Sample	V_{micro} (cm^3g^{-1})	$S_{external}$ (m^2g^{-1})	TIPB cracking conversion (%) [a]	Cumene cracking conversion (%) [b]
Core	0.14	67	79.0	73.7
Coated-3 min	n/d [c]	n/d [c]	48.3	75.1
Coated-5 min	0.14	104	18.4	75.7

a. After pretreating the catalyst in He flow at 300 ℃ for 1 h, the cracking reaction was performed at 1 atm at 400 ℃.

b. After pretreating the catalyst in He flow at 300 ℃ for 1 h, the cracking reaction was performed at 1 atm at 250 ℃.

The outlet stream from the flow reactor was connected to a GC-FID equipped with a silicone SE30 column to quantify the products.

c. No data.

3.3.5 The requirements for ultrafast post-synthesis

Ultrafast direct syntheses of zeolites with various frameworks have been realized benefited from the synergistic effects of seeding, aging, employing high temperature and fast heating.[25] This ultrafast post-synthesis of secondary crystal growth is partially while not total the same as the direct-synthesis case. Despite considerable efforts have been devoted to clarify the effects of various

parameters in accelerating the zeolite synthesis, the seed dissolution proved to be an indispensable step to induce the further crystal growth (as shown in Chapter 2), which is different from the secondary crystal growth of silicalite-1 shell onto the external surface of ZSM-5 core.

There are several factors that have contributed to the successful preparation of core-shell structured ZSM-5@Silicalite-1 zeolite in several minutes: i) the high synthesis temperature and the fast heating; ii) the core zeolite with susceptible external surface; iii) the structural compatibility between the core zeolite and the shell zeolite; iv) the synthesis conditions compatibility between the core zeolite and the shell zeolite. There is no doubt that the high synthesis temperature could accelerate the crystal growth based on an existed surface, as shown in Table 3.2. Additionally, the high temperature could also lead to formation of zeolite phase selectively,[26] thus we could obtain the ZSM-5@Silicalite rather than ZSM-5 and Silicalite-1, separately. The fast heating further allowed a precise control on the ultrafast process because the reaction can be activated and stopped instantly.[27]
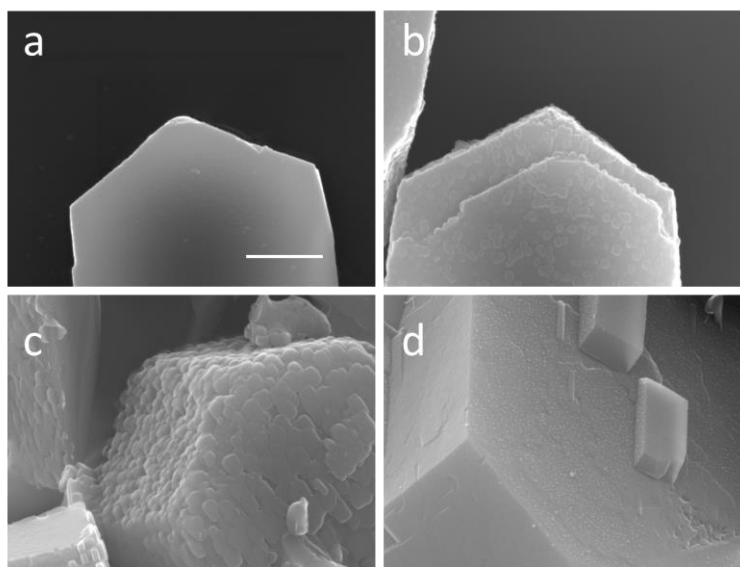
Figure 3.5 SEM images of coated products using commercial ZSM-5 as core for different periods. a, Commercial ZSM-5 zeolite 840 NHA (Si/Al = 19); b) 3 min (Si/Al = 21); c) 5 min (Si/Al = 23); d) 20 min (Si/Al = 26).
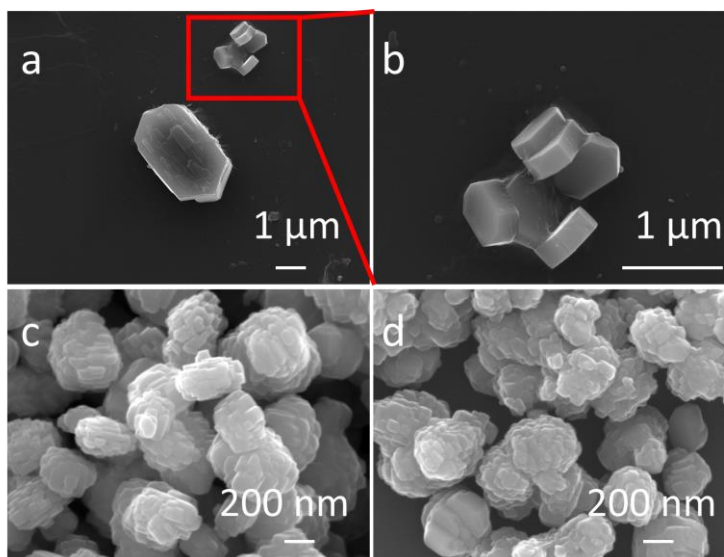
Figure 3.6 SEM images of coated samples obtained through ultrafast coating and conventional coating. a, 840 NHA as core, treated under 150 ℃ for 14 h in autoclave. b, enlargement of square in a, indicating the formation of isolated Silicalite-1. c, as-synthesized ZSM-5 core, treated under 190 ℃ for 5 minute in tubular reactor. d, as-synthesized ZSM-5 core, treated 150 ℃ for 14 h in autoclave.

To examine the effects of ZSM-5 core, a commercial ZSM-5 (840 NHA, TOSOH, Si/Al=20, Figure 3.5a) was used as parent material. Following the same coating procedures, it took 5 min for a full silicalite-1 coverage on the ZSM-5 core (Figure 3.5b and c). However, even the shell thickness and the Si/Al ratio keeps increasing in following 15 minutes and much smoother surface can be observed (Figure 3.5d), the Si source was not used out due to not high enough Si/Al ratio (Si/Al = 26). The long periods needed for treating the commercial zeolites was ascribed to the relatively larger crystal size. Hence, the lower external surface could weaken the interface effects between ZSM-5 core and silicalite-1 synthesis solution. Moreover, when slow heating as well as low synthesis temperature were employed following a conventional route in autoclaves (*e.g.* 150 ℃ for 14 h), large quantities of isolated silicalite-1 crystals were formed simultaneously due to spontaneous nucleation (Figure 3.6a and b). This is similar to the results from previous studies. On the contrary, when the as-synthesized ZSM-5 was used core, either fast preparation or conventional way could prohibit the formation of self-nucleation (Figure 3.6c and d). Therefore, to successfully preparing core-shell structured ZSM-5@Silicalite-1 zeolite, an enhanced interaction between ZSM-5 core and silicalite-1 synthesis solution is needed. Further, the employment of high synthesis temperature not only

accelerates the secondary crystal growth process but also prohibits the self-nucleation of Silicalite-1.
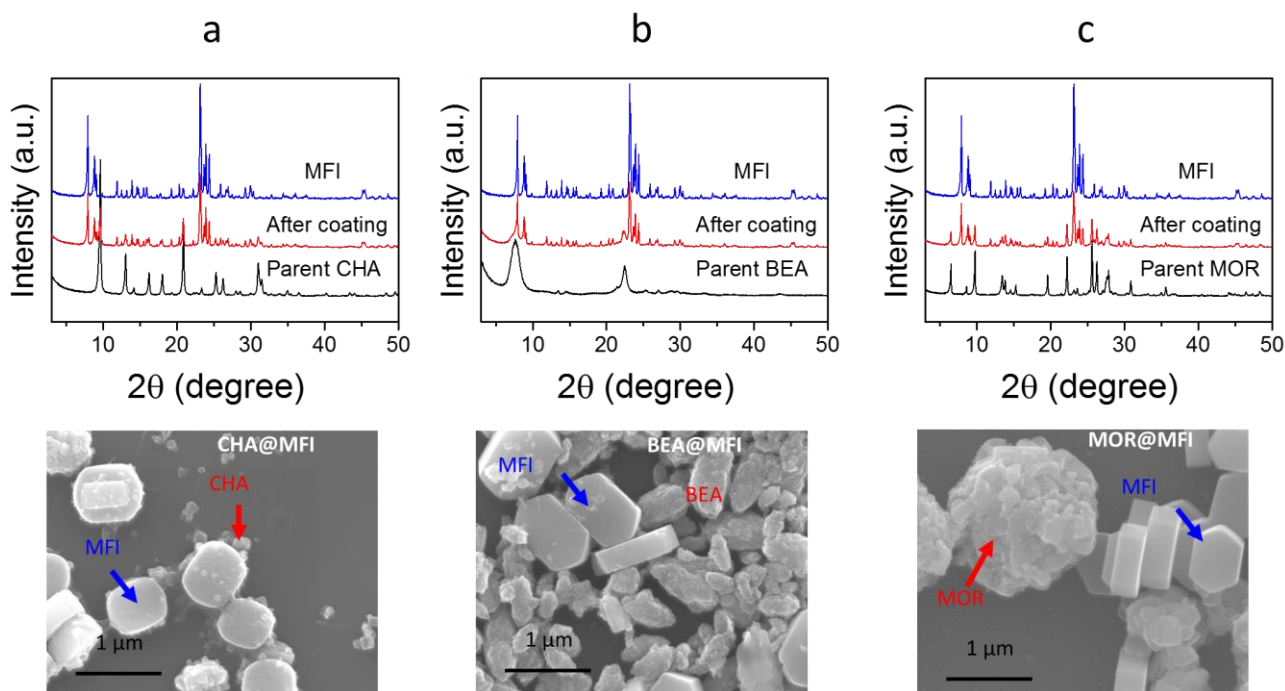
Figure 3.7 XRD patterns and SEM images of the coating results on parent zeolites with different frameworks. a, CHA (SSZ-13, Si/Al = 15.0). b, BEA (Si/Al = 8.0). c, MOR (Si/Al = 6.7).

Three other kinds of zeolites with different frameworks of CHA, BEA, and MOR, were used as cores following the same coating procedures. After 5 minutes of high temperature treatment, neither any silicalite-1 shell was formed but also no formation of isolated silicalite-1 was observed, as confirmed by both of the SEM and XRD analyses. This is much different from the case of using commercial ZSM-5 as core in which, formation of silicalite-1 shell starts soon followed by slow development. A prolonged treatment following the conventional way in autoclaves for longer period was conducted to further clarify these cores' applicability. After 14 h of hydrothermal treatment, mixed XRD peaks assignable to both of core zeolite and silicalite-1 were detected. However, from the SEM images, all newly formed silicalite-1 came out as separated phases from the core crystal (Figure 3.7), different from the case of MFI core in which core-shell structured zeolite was obtained. In previous reports, for core-shell structured zeolites with different core and shell zeolites, beforehand deposition of nanocrystalline seeds of shell zeolite is needed to induce the further secondary growth on the surface of core zeolite.[11] Thus, a structural similarity between the core zeolite and shell zeolite is a crucial factor which contributes to the fast preparation of core-shell structured zeolites.
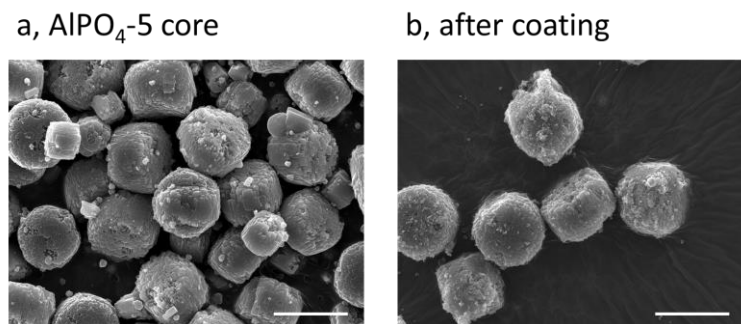
Figure 3.8 SEM images of AlPO$_4$-5 zeolite (a) and the product after coating treatment under 210 ℃ for 3 h. (Scale bar = 5 μm)

Last but not the least, though the shell zeolite may take the same framework as core zeolite, the mismatch between their syntheses conditions lead to unsuccessful formation of core-shell structured zeolites. In a recent study, SSZ-24 zeolite having the AFI framework was successfully synthesized in 60 minutes, which was a remarkable improvement since 18 days were needed in conventional synthesis. Such kind of fast crystallization of SSZ-24 zeolite made it a possible candidate for growing on a zeolite core having the same framework, namely, AlPO$_4$-5 zeolite. However, none of the efforts proved be effective even all the other parameters like high temperature, fast heating, seeding or the same structures of core and shell zeolites seemed be fulfilled. Instead of forming a core-shell structured zeolite, increase in neither of crystal size nor solid yield was observed, thus suggesting an unsuccessful growth of SSZ-24 on the surface of core AlPO$_4$-5 zeolite. Therefore, to form a core-shell structured zeolite in an ultrafast post-synthesis way, very careful adjustment on the reaction conditions should be considered.

Overall, the ultrafast post-synthesis for core-shell structured zeolites was realized by combining several favorable factors. This ultrafast post-synthesis not only provides a more efficient way for producing a kind of functional materials, but also allows a more precise way to investigate the interaction between crystalline parent zeolite and the treating liquor solutions. This latter benefit is expected to be significant in clarifying the structural flexibility of crystalline zeolites toward more effective post-synthesis modifications.

3.3.6 Continuous flow synthesis system built for core-shell structured zeolites

Although the ultrafast post-synthesis for core-shell structured zeolites has been realized in

several minutes by using a batched, tubular reactor, the exhausted operations on start-up and shut-down always present as drawbacks for improving the production efficiency practically. Developing continuous flow reaction system, will be effective to overcome above mentioned limitations. Continuous flow synthesis have been extensively applied in many fields such as pharmaceuticals and fine chemicals chemistry. In the previous studies of our group, the synthesis of zeolites can be also realized when considerable efforts are devoted in adjusting the conditions among kinetics, thermodynamics, and hydrodynamics perspectives. Despite such kind of significant improvement in prompting the efficient production of crystalline microporous materials, establishing a continuous flow synthesis system applicable for producing functional zeolite materials through ultrafast post-synthesis is still a challenge because of the higher complexity and ambiguity in a mixed liquid-solid fluid. The parent materials used in the post-synthesis treatment is significantly different from the seed used in a direct-synthesis route since no obvious dissolution is allowed while instead, in this case, shell zeolite should rapidly grow on the surface of core zeolite. Thus, a well balance for the interface interaction effect should be carefully reached for a successful crystal growth under continuous flowing condition.
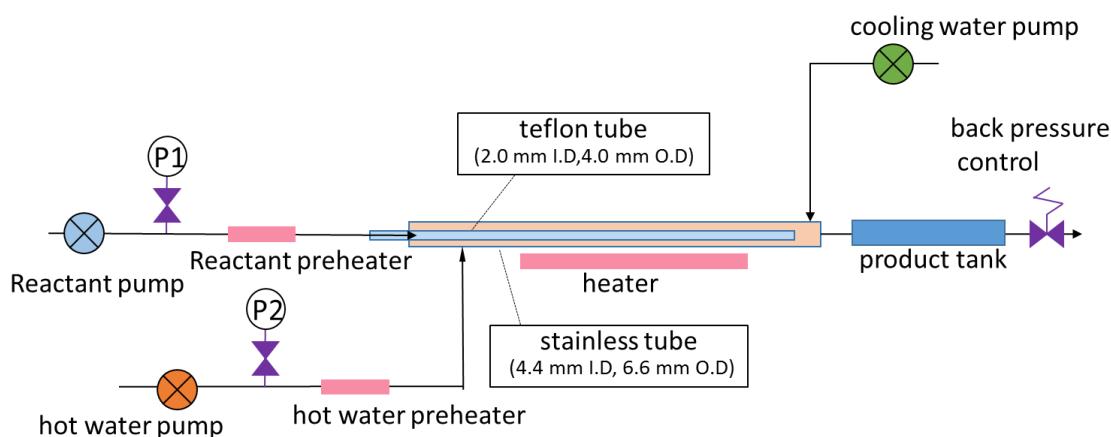
Scheme 3.1 Schematic illustration of the continuous flow reaction system for preparing core-shell zeolites

There are several advantages of using continuous flow synthesis: i) fast mixing of the reagents, ii) enhanced mass transfer efficiency between different phases (liquid, gas, solid), iii) high temperature treatment with much shortened cryogenic conditions, iv) facile control on the residence

time by changing the reactor length or fluid speed. In the ultrafast flow preparation of core-shell structured ZSM-5@Silicalite-1 case, a parallel two-tubes system including an inner Teflon® (*o.d./i.d.* = 4.0/2.0 mm) tube and an outer stainless (*o.d./i.d.* = 6.6/4.4 mm) tube was used. The well mixed reactant was transferred into the inner tube with the assistance of a high pressure syringe pump, while hot water was fed into the outer tube for a fast, uniform heating and further high temperature treatment. At the end the reactor, where blockage occurs easily due to the precipitation of products, cooling water was pumped in to dilute and cool the reaction fluid. A typical illustration of this continuous flow reaction system for core-shell structured zeolite is shown in Scheme 3.1.
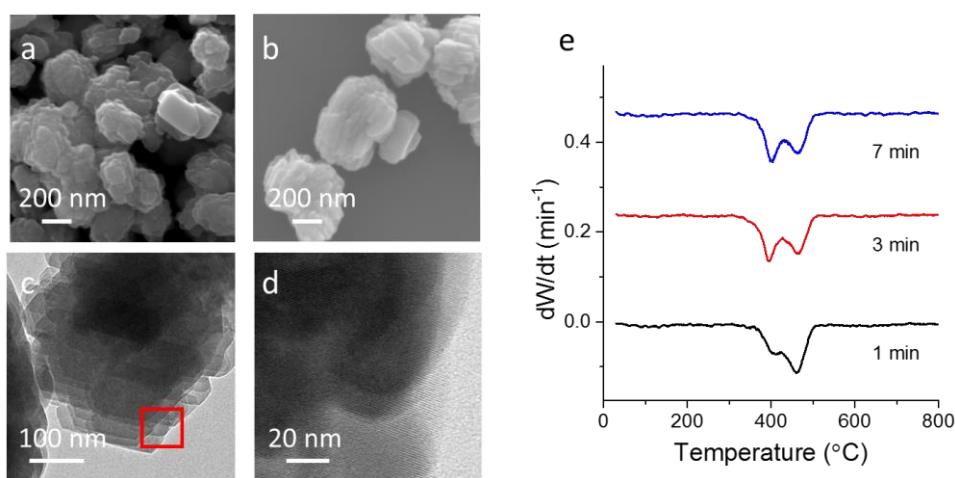
Figure 3.9 Core-shell structured ZSM-5@Silicalite-1 prepared in a continuous flow reaction system. a, SEM images of ZSM-5 core (Si/Al = 26). b, SEM image of coated-3 min (Si/Al = 46). c, TEM images of coated-3 min. d, High resolution TEM image (red square in c). e, DTG curves of the coated samples for different periods.

The coating process in the flow system reached the saturation point in 3 min with the constant Si/Al ratio and crystal size (Figure 3.9a and b). The even faster crystal growth rate than that of using batched tube reactor is attributed to the higher heat transfer efficiency as well as the greater surfaceto-volume ratio of thinner tubular reactors. TEM images of the sample coated for 3 min indicate that the core-shell product has a crystalline shell of silicalite-1 crystals (Figure 3.9 c and d), similar to the results of using batched tubular reactor. The earlier appearance and faster development of the DTG peak assigned to loss of TPA^+ located in silicalite-1 shell further confirmed that the core-shell structured ZSM-5@Silicalite-1 could be produced in an established continuous flow reaction system

efficiently.

3.4 Summary

An ultrafast post-synthesis coating treatment capable of producing core-shell structured ZSM-5@Silicalite-1 in several minutes was demonstrated in this chapter. Through this treatment, the surface acidity, an important factor governing the catalytic performance of zeolite catalysts can be precisely controlled in such a short period. Typically effective parameters in hydrothermal process such as temperature, reagent composition also showed considerable effects on this fast preparation. The successful preparation of the core-shell structured zeolite in an ultrashort period was originated from several synergistic factors including high treatment temperature, reactor featuring fast heating, and structural compatibility between core and shell zeolites. Moreover, a continuous flow reaction system was developed to replica this ultrafast preparation, and the period requested for saturating the coating treatment could be further shortened thanks to the even faster heating transfer as well as mixing efficiency.

Compared with the direct-synthesis, post-synthesis treatment showed superiority in tailoring the zeolite properties in a more economical and versatile way. Considering the potential in large-scaled production of functional zeolitic materials with various desired properties, this ultrafast fast post-synthesis for core-shell structured zeolite is possible to open a new insight on developing more practical and efficient strategy for promoting the industrialization new zeolite materials.

References

[1]   B. Smit, T.L. Maesen, Towards a molecular understanding of shape selectivity, *Nature* **2008**, 451, 671.

[2]   Y. Wang, J. Zhuang, G. Yang, D. Zhou, D. Ma, X. Han, X. Bao, Study on the external surface acidity of MCM-22 zeolite: Theoretical calculation and 31P MAS NMR, *J. Phys. Chem. B* **2004**, 108, 1386-1391.

[3]   L.D. Rollmann, ZSM-5 containing aluminum-free shells on its surface, U.S. Pat., US4088605A, **1978**.

[4]   Y.T. Cheng, Z. Wang, C.J. Gilbert, W. Fan, G.W. Huber, Production of p‑xylene from biomass by catalytic fast pyrolysis using ZSM‑5 catalysts with reduced pore openings, *Angew. Chem. Int. Ed.* **2012**, 51, 11097-11100.

[5]   M. Niwa, S. Kato, T. Hattori, Y. Murakami, Fine control of the pore-opening size of the zeolite mordenite by chemical vapour deposition of silicon alkoxide, *J. Chem. Soc. Faraday Trans.* **1984**, 80, 3135-3145.

[6]   K. Tominaga, S. Maruoka, M. Gotoh, N. Katada, M. Niwa, HZSM-5 modified by silica CVD for shape-selective production of p-xylene: Influence of in situ and ex situ preparation conditions of the zeolite, *Micropor. Mesopor. Mater.* **2009**, 117, 523-529.

[7]   R.W. Weber, J. Fletcher, K. Möller, C. O'Connor, The characterization and elimination of the external acidity of ZSM-5, *Micropor. Mater.* **1996**, 7, 15-25.

[8]   J. Kim, H.S. Kim, N. Lee, T. Kim, H. Kim, T. Yu, I.C. Song, W.K. Moon, T. Hyeon, Multifunctional uniform nanoparticles composed of a magnetite nanocrystal core and a mesoporous silica shell for magnetic resonance and fluorescence imaging and for drug delivery, *Angew. Chem. Int. Ed.* **2008**, 47, 8438-8441.

[9]   P. Reiss, M. Protiere, L. Li, Core/shell semiconductor nanocrystals, *small* **2009**, 5, 154-168.

[10]   S. Chen, Z. Wei, X. Qi, L. Dong, Y.-G. Guo, L. Wan, Z. Shao, L. Li, Nanostructured polyaniline-decorated Pt/C@ PANI core–shell catalyst with enhanced durability and activity, *J. Am. Chem. Soc.* **2012**, 134, 13252-13255.

[11]   Y. Bouizi, I. Diaz, L. Rouleau, V.P. Valtchev, Core–shell zeolite microcomposites, *Adv. Funct. Mater.* **2005**, 15, 1955-1960.

[12]   T. Okubo, T. Wakihara, J. Plévert, S. Nair, M. Tsapatsis, Y. Ogawa, H. Komiyama, M. Yoshimura, M.E. Davis, Heteroepitaxial growth of a zeolite, *Angew. Chem. Int. Ed.* **2001**, 40, 1069-1071.

[13]   T. Wakihara, S. Yamakita, K. Iezumi, T. Okubo, Heteroepitaxial growth of a zeolite film with a patterned surface-texture, *J. Am. Chem. Soc.* **2003**, 125, 12388-12389.

[14]   Y. Bouizi, L. Rouleau, V.P. Valtchev, Bi-phase MOR/MFI-type zeolite core–shell composite, *Micropor. Mesopor. Mater.* **2006**, 91, 70-77.

[15]   J. Zheng, X. Zhang, Y. Wang, Y. Bai, W. Sun, R. Li, Synthesis and catalytic performance of a bi-phase core-shell zeolite composite, *J. Porous Mater.* **2009**, 16, 731.

[16]   G.D. Pirngruber, C. Laroche, M. Maricar-Pichon, L. Rouleau, Y. Bouizi, V. Valtchev, Core–shell zeolite composite with enhanced selectivity for the separation of branched paraffin isomers, *Micropor. Mesopor. Mater.* **2013**, 169, 212-217.

[17]   B. Ren, S. Bai, J. Sun, F. Zhang, M. Fan, Controllable synthesis of obvious core–shell structured Y/Beta composite zeolite by a stepwise-induced method, *RSC Adv.* **2014**, 4, 22755-22758.

[18]   A. Ghorbanpour, A. Gumidyala, L.C. Grabow, S.P. Crossley, J.D. Rimer, Epitaxial growth of ZSM-5@ Silicalite-1: A core–shell zeolite designed with passivated surface acidity, *ACS nano* **2015**, 9, 4006-4016.

[19]   C. Peng, Z. Liu, A. Horimoto, C. Anand, H. Yamada, K. Ohara, S. Sukenaga, M. Ando, H. Shibata, T. Takewaki, Preparation of nanosized SSZ-13 zeolite with enhanced hydrothermal stability by a two-stage synthetic method, *Micropor. Mesopor. Mater.* **2018**, 255, 192-199.

[20]   L. Young, S. Butter, W. Kaeding, Shape selective reactions with zeolite catalysts: III. Selectivity in xylene isomerization, toluene-methanol alkylation, and toluene disproportionation over ZSM-5 zeolite catalysts, *J. Catal.* **1982**, 76, 418-432.

[21]   M. Miyamoto, T. Kamei, N. Nishiyama, Y. Egashira, K. Ueyama, Single Crystals of ZSM‐5/Silicalite Composites, *Adv. Mater.* **2005**, 17, 1985-1988.

[22]   C. Peng, Z. Liu, Y. Yonezawa, Y. Yanaba, N. Katada, I. Murayama, S. Segoshi, T. Okubo, T. Wakihara, Ultrafast post-synthesis treatment to prepare ZSM-5@ Silicalite-1 as a core-shell structured zeolite catalyst, *Micropor. Mesopor. Mater.* **2019**, 277, 197-202.

[23]   J. Hedlund, S. Mintova, J. Sterte, Controlling the preferred orientation in silicalite-1 films

synthesized by seeding, *Micropor. Mesopor. Mater.* **1999**, 28, 185-194.

[24] M. Niwa, N. Katada, Y. Murakami, Thin silica layer on alumina: evidence of the acidity in the monolayer, *J. Phys. Chem.* **1990**, 94, 6441-6445.

[25] Z. Liu, J. Zhu, T. Wakihara, T. Okubo, Ultrafast synthesis of zeolites: breakthrough, progress and perspective, *Inorg. Chem. Front.* **2019**, 6, 14-31.

[26] Z. Liu, T. Wakihara, N. Nomura, T. Matsuo, C. Anand, S.P. Elangovan, Y. Yanaba, T. Yoshikawa, T. Okubo, Ultrafast and continuous flow synthesis of silicoaluminophosphates, *Chem. Mater.* **2016**, 28, 4840-4847.

[27] Z. Liu, T. Wakihara, C. Anand, S.H. Keoh, D. Nishioka, Y. Hotta, T. Matsuo, T. Takewaki, T. Okubo, Ultrafast synthesis of silicalite-1 using a tubular reactor with a feature of rapid heating, *Micropor. Mesopor. Mater.* **2016**, 223, 140-144.

[28] C. Peng, Z. Liu, Y. Yonezawa, Y. Yanaba, N. Katada, I. Murayama, S. Segoshi, T. Okubo, T. Wakihara, Ultrafast post-synthesis treatment to prepare ZSM-5@ Silicalite-1 as a core-shell structured zeolite catalyst, *Micropor. Mesopor. Mater.* **2019**, 277, 197-202.

Chapter 4 Ultrafast Desilication and Surfactant-templating for Mesostructured Zeolites

「 ゼオライトの高機能化に向けた高速合成及び後処理手法の開発」 という博士論文の一部 である第

4 章は雑誌掲載の形で刊行される予定で、全文公表はできない。

具体的に、「 Angewandte Chemie International Edition」および「 Microporous and Mesoporous

Materials」に投稿する予定である。

Chapter 5 General Conclusions and Future Perspectives

5.1 General conclusions

The modern zeolite chemistry has been developed for several decades, along with which, not only the zeolite structures which can be artificially synthesized are increased, but also potential applications of zeolite materials in emerging sustainable chemistry processes are intensified. However, a main challenge which limits the practical applications of zeolite materials is still the zeolite synthesis. How to efficiently prepare zeolite materials with desired properties is an urgent topic to be studied so as to prompt the industrialization of zeolite materials.

In chapter 1, an overview background on the relation among structures, applications and synthesis of zeolite materials is presented firstly. Continuous flow chemistry has thought to be an advanced step to enhance the efficiency of producing zeolite materials. Several examples of synthesizing zeolites on the order of minutes show the high potential of continuous production of zeolite materials based on the ultrafast synthesis strategy. In this strategy, seeding and aging effects, employing high synthesis temperatures and reactors featuring fast heating are decisive parameters. Nevertheless, very little attention was paid to how the ultrafast strategy could influence the zeolite structures. An objective of preparing functional zeolite materials with desired properties in an ultrafast way is proposed. For introducing desired properties in zeolite structures, both direct-synthesis and post-synthesis modifications have been taken into considerations, which corresponds to the title of this thesis "Developing ultrafast methods of synthesis and post-synthesis modification toward highly functionalized zeolite materials".

In Chapter 2, direct-synthesis of nanosized SSZ-13 zeolite with enhanced hydrothermal stability was investigated through a two-stage synthetic way under different temperature programs. The first low-temperature stage (95 ℃, 0–24 h) showed substantial effects determine the amounts of the nuclei formed before crystal growth; the high-temperature stage (210 ℃, 5–60 min) allowed the crystal growth finished in several minutes. Resultantly, nanosized SSZ-13 zeolite was obtained with facilely controllable ranges of 50–300 nm. Moreover, the high-temperature stage not only accelerated the crystal growth, but also helped heal the intrinsic defects formed in the previous low-

temperature stage. Compared with the micronsized SSZ-13 zeolite obtained through a conventional way (150 ℃, 48 h) or nanosized counterpart obtained after saturated synthesis under low-temperature (95 ℃, 72 h), the nanosized SSZ-13 prepared by the fast way showed remarkably enhanced hydrothermal stability.

In chapter 3, an ultrafast post-synthesis modification for preparing core-shell structured zeolite catalyst was achieved in 5 minutes under high temperature of 190 ℃. The surface acidity of zeolite catalysts is often undesired for possible non-selective side reactions. Growing an inert shell (Silicalite-1) on the active surface of zeolite core (ZSM-5) was proved to be effective to reduce the surface active sites, as confirmed by catalyzing the cracking of large molecules (TIPB). The thickness of the shell part being important to adjust the surface acidity was facilely controllable by changing the treating periods, reaction compositions and temperatures. Compared with traditionally method for preparing core-shell structured zeolites in under low temperatures for long periods (150 ℃, 14 h), the ultrafast method not only provide an efficient way for tailoring the active sites but also showed superior selection on avoiding the formation of isolated shell zeolite other than core-shell structure.

In chapter 4, ultrafast surfactant-assisted alkaline treatments including both of ultrafast desilication and ultrafast surfactant-templating were demonstrated to efficiently introduce mesoporosity in microporous zeolites. The employment of high treatment temperatures and use of tubular reactor featuring fast heating had accelerated the alkali etching effects on the parent zeolites remarkably, while the addition of surfactants could allow a controllable mesostructuring process steadily. Using ZSM-5 zeolite as parent material, ultrafast desilication has been realized in 3 minutes to introduce large amounts of mesopores (V_{meso}=0.58 cm^{3}g^{-1}, $S_{external}$=310 m^{2}g^{-1}). When USY zeolite was used as parent material, the ultrafast surfactant-templating for introducing saturated mesoporosity can be achieved in just 1 minute following a local structure re-construction mechanism. A kinetic study on the ultrafast surfactant-templating treatment (150–220 ℃, 0–5 min) was proceeded, resulting the calculated apparent activation energy of 29 kJ·mol^{-1}. This result is comparable to the crystallization of zeolite structures and the generally low-temperature surfactant-templating processes, indicating the feasibility of the ultrafast formation of the mesoporous zeolite. The amounts and/or sizes of the mesopores created through this ultrafast strategy can be easily controlled by changing the initial alkaline concentration and/or the conditions of surfactants

including amounts and species.

Ultrafast syntheses have been reported to be reproducible in continuous flow reaction systems. Considering the difference between the direct-synthesis and post-synthesis, improvements on the continuous flow reactor were made to accommodate an appropriate condition for corresponding post-synthesis modification. Consequently, the preparation of core-shell structured zeolite through ultrafast secondary growth, as well as the introduction of mesoporosity in zeolites through alkaline treatments are also achieved in continuous flow reactors.

In conclusion, this thesis demonstrates the successful developments of ultrafast strategy in introducing desired properties in zeolite products through either direct-synthesis or post-synthesis modification. Realizing such kinds of ultrafast preparation of functional zeolite materials is of highly valuable from both of i) fundamental aspect that how fast the creation or re-arrangement of zeolite structures under hydrothermal conditions could be achieved and ii) practical aspect that a more efficient and economical way for functional zeolite materials could be expected. Consequently, the main contributions of this thesis are as follows: first of all, the ultrafast post-syntheses of tailoring the zeolite structures for desired acidity distribution and pore system were achieved in several minutes, indicating a surprisingly structural flexibility of existed zeolites to accommodate the improved properties. The kinetic study had proved the feasibility of the ultrafast post-synthesis modifications as the traditionally hydrothermal synthesis of zeolites. More importantly, continuous flow reaction systems were established to reproduce the ultrafast tailoring of the zeolite properties, which can be a great progress to prompt the industrial production of functional zeolite materials.

5.2 Future perspectives

The practical applications of zeolite materials are closely related to their production efficiency, due to which, tremendous efforts have been devoted to accelerate the zeolite synthesis, as described in the Introduction part. Based on the previously develop ultrafast strategy for synthesizing zeolites in several minutes, this thesis demonstrate a further development of the ultrafast strategy for producing functional zeolite materials with desired properties in the ways not only limited in the direct-synthesis, but rather, post-synthesis modifications are also included.

Several typical examples of tailoring the important properties of zeolite catalysts on the order of minutes, for instance, crystal size, hydrothermal stability, acid sites distribution, and hierarchical pore structures, were presented in this thesis. These successful cases further allowed to develop the continuous production of the functional zeolite materials.

Considering the diversity of zeolite structures, future efforts based on this doctoral work can be located on widening the applicable ranges of the ultrafast strategy for different kinds of zeolites. This target should be addressed by taking several issues into consideration: i) understanding the changes of different species during the interaction between solid zeolites and liquid treating solutions, for example, the Si/Al ratio in the solid and the liquid phase; ii) clarifying the possible driving force for structural variations, for which, variation of the interface properties should be taken into consideration; iii) differentiating the stability of various zeolite structures in hot aqueous environment because of the significant difference compare with the thermal and/or hydrothermal stability. On the other hand, to build a pilot factory for enlarging the production of the functional zeolite materials, the fluidic chemistry of the mixture of zeolite solids and treatment aqueous should be studied comprehensively.

Acknowledgement

Part of the results described in this thesis are benefited from the assistance of several persons to whom I want to thank: Prof. H. Shibata, Prof. S. Sukenaga, Ms. M. Ando, and Mr. Y. Yutaka for solid-state NMR analysis, Prof. A. Endo and Mr. T. Matsumoto for CP-SEM analysis, Dr. H. Yamada and Dr. K. Ohara for HEXTS analysis.

I also thank the senior and fellow lab-mates for the stimulating discussions: Dr. Le Xu, Dr. Natsume Koike, Dr. Takenori Iida, Dr. Koki Muraoka, Dr. Sye Hoe Keoh, Miss Che Tan, Miss Jie Zhu, Miss Menghe Xu, Mr. Peidong Hu, and Mr. Jingtian Chen. In this Japanese research group, I have also received many kind helps from all the people around. I would like to thank Prof. Kenta Iyoki and Prof. Wei Fan for fruitful discussions. I thank all the secretaries for their kind address on all the issues during my lab daily life: Ms. Kazuko Yokoyama, Ms. Keiko Kotani, Ms. Tomoko Yoshihara, Ms. Naomi Minamoto, Ms. Akiyo Yoshimori, Ms. Chika Noguchi. All in all, without the help from all the members in Okubo-Wakihara laboratory, I cannot proceed my doctoral periods smoothly in the past three years.

Last but not the least, I would like to thank my family: my wife, my parents, and my brother for their unconditional love and continuous support. My wife, Dr. Mingwei Mu came to Japan 1 year earlier than me. She went through so many difficulties by herself alone in Japan and created a much more stable environment for my doctoral study. I appreciate all the efforts she had paid for me and would like to promise her a forever support.

List of Publications

Publication related to this thesis

[1]   Peng C., Liu Z., Horimoto A., Anand C., Yamada H., Ohara K., Sukenaga S., Ando M., Shibata H., Takewaki T., Mukti R.R., Okubo T, and Wakihara T., "Preparation of nanosized SSZ-13 zeolite with enhanced hydrothermal stability by a two-stage synthetic method" *Micropor. Mesopor. Mater. 255*, 192-199 (2018) (Chapter 2)

[2]   Peng C., Liu Z., Yonezawa Y., Yanaba Y., Katada N., Murayama I., Segoshi S., Okubo T. and Wakihara T., "Ultrafast post-synthesis treatment to prepare ZSM-5@ Silicalite-1 as a core-shell structured zeolite catalyst" *Micropor. Mesopor. Mater. 277*, 197-202 (2019) (Chapter 3)

[3]   Peng C., Liu Z., Yonezawa Y., Linares N., Yanaba Y., Trujillo A.C., Okubo T., Taiji Matsumoto, Garc á-Martínez J., Wakihara T., "Testing the limits of zeolite structural flexibility: Introducing mesoporosity in zeolites in just 1 min" Submitted (Chapter 4)

[4]   Peng C., Liu Z., Yonezawa Y., Okubo T., Wakihara T., "Ultrafast synthesis as a highly efficient strategy to promote the desilication process" in preparation (Chapter 4)

Other publications

[1]   Peng C., Liu Z., Okubo T. and Wakihara T., "Fast synthesis of SSZ-24: A pure silica zeolite with AFI framework" *Chem. Lett. 47*, 654-656 (2018)